nature communications

Article

https://doi.org/10.1038/s41467-025-57490-6

RNA-binding proteins DND1 and NANOS3 cooperatively suppress the entry of germ cell lineage

Received: 30 July 2024

Accepted: 24 February 2025

Published online: 23 May 2025

Check for updates

Ziqi Wang[1,12], Honglin Yu[1,2,12], Zhaoyu Gu[1], Xiaohui Shi[1], Jiayue Ma[1], Qizhe Shao[1], Yao Yao[1], Shuo Yao[1], Yan Xu[1], Yashi Gu[1,2], Jiayue Dai[1,2], Qi Liu[1], Jingyan Shi[1], Rujie Qi[1], Yue Jin[2,3], Yuqian Liu[2,3], Xinchen Shen[1], Wenwen Huang[1], Heng-Jia Liu[2,3], Min Jin[4], Wanlu Liu[5,6,7,8], Matthew Brook[9] ✉ & Di Chen[1,2,10,11] ✉

Specification of primordial germ cells (PGCs) establishes germline development during early embryogenesis, yet the underlying mechanisms in humans remain largely unknown. Here, we reveal the functional roles of germline-specific RNA-binding protein (RBP) DND1 in human PGC (hPGC) specification. We discovered that DND1 forms a complex with another RBP, NANOS3, to restrict hPGC specification. Furthermore, by analyzing the mRNAs bound by DND1 and NANOS3, we found that DND1 facilitates the binding of NANOS3 to hPGC-like cells-related mRNAs. We identified *SOX4* mRNAs as the key downstream factor for the DND1 and NANOS3 complex. Mechanistically, DND1 and NANOS3 function in processing bodies (P-bodies) to repress the translation of *SOX4* mRNAs, with NANOS3 mediating the interaction between DND1 and the translational repressor 4E-T. Altogether, these findings identify the RBP complex formed by DND1 and NANOS3 functioning as a "braking system" to restrict the entry of germ cell fate in humans.

The reproductive lineage originates from primordial germ cells (PGCs), the precursors to sperm and eggs[1,2]. PGCs are responsible for re-establishing totipotency and are critical for the transmission of genetic and epigenetic information across generations, forming the basis for sexual reproduction. PGC specification marks the beginning of reproductive system development, and defects in this process may lead to infertility, germ cell tumors, and other severe diseases such as birth defects. Deciphering the regulatory networks governing human

[1]Center for Reproductive Medicine of The Second Affiliated Hospital, Center for Regeneration and Cell Therapy of Zhejiang University-University of Edinburgh Institute (ZJU-UoE Institute), Zhejiang University School of Medicine, Zhejiang University, Haining, Zhejiang, China. [2]Edinburgh Medical School: Biomedical Sciences, College of Medicine and Veterinary Medicine, The University of Edinburgh, Edinburgh, UK. [3]Center for Infection Immunity and Cancer, Zhejiang University-University of Edinburgh Institute (ZJU-UoE Institute), Zhejiang University School of Medicine, Zhejiang University, Haining, Zhejiang, China. [4]Center for Reproductive Medicine of The Second Affiliated Hospital, Zhejiang University School of Medicine, Zhejiang University, Hangzhou, Zhejiang, China. [5]Department of Orthopedic Surgery of the Second Affiliated Hospital, Zhejiang University School of Medicine, Zhejiang University, Hangzhou, Zhejiang, China. [6]Center of Biomedical Systems and Informatics of Zhejiang University-University of Edinburgh Institute (ZJU-UoE Institute), International Campus, Zhejiang University, Haining, Zhejiang, China. [7]Future Health Laboratory, Innovation Center of Yangtze River Delta, Zhejiang University, Jiaxing, China. [8]Alibaba-Zhejiang University Joint Research Center of Future Digital Healthcare, Zhejiang University, Hangzhou, Zhejiang, China. [9]Centre for Cardiovascular Science, Queen's Medical Research Institute, University of Edinburgh, Edinburgh, Scotland, UK. [10]State Key Laboratory of Biobased Transportation Fuel Technology, Haining, Zhejiang, China. [11]Dr. Li Dak Sum & Yip Yio Chin Center for Stem Cell and Regenerative Medicine, Zhejiang University, Hangzhou, Zhejiang, China. [12]These authors contributed equally: Ziqi Wang, Honglin Yu. ✉e-mail: matt.brook@ed.ac.uk; dichen@intl.zju.edu.cn

PGC (hPGC) specification is crucial for mechanistic understanding of germ cell development and pathogenetic investigation of germ cell-related diseases.

Historically, mice have served as the model organism for understanding human germ cell development[3–6], providing fundamental insights into the specification and differentiation of hPGCs. However, recently established in vitro hPGC-like cell (hPGCLC) induction models based on pluripotent stem cells have revealed that human PGC specification is not as conserved as previously expected[7–9]. For example, the specification of mouse PGCs (mPGCs) is determined by the transcription factors PRDM1, PRDM14, and TFAP2C, among which PRDM14 is the most essential cell fate determinant[10,11]. Overexpression of PRDM14 alone is sufficient to induce the specification of mPGCs from competent embryonic cells[11]. Meanwhile, SOX2 is another critical transcription factor for mPGCs[12]. However, PRDM14 functions differentially in hPGCLCs[7,8], SOX2 is not expressed in hPGCs, while TFAP2C and SOX17 are critical for establishing human germ cell programs[8,13]. These species-differences emphasize the importance of investigating human PGC specification and development using hPGCLC induction system.

In addition to transcriptional regulation, post-transcriptional modulation mediated by RNA-binding proteins (RBPs) is critical for germ cell development[14,15]. It has been recognized that RBPs exhibit cell-type specific expression patterns[16], for example, RBPs such as DND1[17,18], NANOS3[19,20], and DDX4[21,22], are specifically expressed in germ cells. However, how these germ cell-specific RBPs regulate the specification of hPGCs is not fully understood. As one of the typical germ cell-specific RBPs, DND1 has been extensively studied in model organisms[23]. Knock-down of *Dnd* in zebrafish results in failure of PGC migration and trans-differentiation of PGCs into somatic cells[24]. Knock-out of *Dnd1* in mice leads to defects in PGC migration and spermatogonial differentiation[17,25]. DND1 may play cell-stage-specific roles during germ cell development by interacting with different partners[23,26]. Moreover, DND1 binds to the 3' untranslated regions (3'UTR) of its target mRNAs to protect them from miRNA-mediated translational repression[27]. Besides, DND1 can interact with CCR4-NOT complex to facilitate the degradation of target mRNAs[28]. However, the mechanisms through which DND1 regulates the specification and development of human PGCs remain largely elusive.

Understanding the molecular functions of DND1 is crucial not only for deciphering the RBP-mediated post-transcriptional regulation of germ cell development, but also for investigating germ cell-related diseases. Some mutations in the *DND1* gene have been linked to non-obstructive azoospermia[29], underscoring the importance of elucidating the molecular mechanisms through which DND1 regulates human germ cell development. Although DND1 has been used as one of the hPGC markers, and a few studies have explored its functions in humans[30], the molecular functions of DND1 in hPGC specification are not fully addressed. RBPs tend to function as ribonucleoprotein complexes for regulating their target mRNAs[31]. In a related study, Co-Immunoprecipitation Mass Spectrometry (co-IP-MS) analysis of DND1 in HEK293 cells identified NANOS3 as an interacting protein for DND1[28]. NANOS3 is also an evolutionarily conserved RBP that plays key roles for PGC development in model organisms[17,19,20,32]. Mutations in *NANOS3* have been associated with premature ovarian failure in human women[33,34]. Nonetheless, how DND1-based RBP complex is involved in the regulation of hPGC specification and development remains to be determined.

In this study, we identified that DND1 and its interacting partner NANOS3 as an RBP complex that restricts the specification of hPGCLCs induced from human embryonic stem cells (hESCs). DND1 is required for NANOS3 to bind to their target mRNAs, while NANOS3 is required for DND1 to interact with 4E-T in P-bodies for translational regulation, to coordinate germ cell development by suppressing the translation of *SOX4*.

Results

DND1 restricts the specification of primordial germ cells induced from human embryonic stem cells

To understand the RNA-binding protein (RBP)-mediated post-transcriptional regulation of germ cell development, we interrogated the requirement for and functions of the RBP DND1 (D1) in human germline specification from hESCs. Guide RNAs (gRNAs) were designed to delete all coding sequence from the *D1* gene (Fig. 1A; Supplementary Fig. 1A). The *D1* knock-out (*D1-KO*) hESCs could be maintained for more than 30 passages, with comparable morphology and karyotype to that of control hESCs (Fig. 1B; Supplementary Fig. 1B). Importantly, the expression of pluripotency genes, including *POU5F1* (*OCT4*), *NANOG*, and *SOX2*, was comparable between *D1-KO* and control hESCs (Supplementary Fig. 1C), and *D1-KO* hESCs were positive for NANOG and OCT4 by immunofluorescence (Supplementary Fig. 1D). Additionally, *D1-KO* hESCs were positive for the pluripotency marker SSEA4 by flow cytometry (Supplementary Fig. 1E). These results indicate that D1 is not required for the maintenance of hESCs.

Next, we detected whether D1 regulates the differentiation of hESCs by forming embryoid bodies (Supplementary Fig. 1F). We found that the expression levels of differentiation markers for endoderm (*GATA4, GATA6*, and *SOX17*), mesoderm (*T, EVX1, SP5, MIXL1, MSX2*, and *NODAL*), and ectoderm (*PAX6*) were up-regulated in embryoid bodies derived from *D1-KO* hESCs, while the expression of pluripotency markers *NANOG* and *POU5F1* was decreased (Supplementary Fig. 1G). Flow cytometry using antibodies against Annexin V showed that the percentage of dead cells was comparable between *D1-KO* and control hESCs (Supplementary Fig. 1H). Finally, we performed RNA-sequencing (RNA-seq) on *D1-KO* hESCs. There were 248 up-regulated and 391 down-regulated differentially expressed genes (DEGs) in *D1-KO* hESCs compared to controls (Supplementary Fig. 1I; Supplementary Data 1). Gene Ontology (GO) term analysis indicated that urogenital system development was the most significantly down-regulated biological process in *D1-KO* hESCs (Supplementary Fig. 1I; Supplementary Data 1). Together, these observations indicate that D1 is not required for the maintenance and pluripotency of hESCs.

Next, we aimed to determine whether D1 is involved in the regulation of hPGCLCs induced from hESCs. First, we verified the deletion of *D1* by qPCR analysis of the expression of *D1* mRNAs in day 4 hPGCLC aggregates (Fig. 1C). We then examined the induction of hPGCLCs during 8 days of aggregate culture. Interestingly, we found that the percentage of hPGCLCs increased in *D1-KO* aggregates compared to controls (Fig. 1D, G), suggesting that D1 functions to restrict hPGCLC specification.

Given that the observed phenotype is inconsistent with findings in model organisms such as mice[35] and zebrafish[36], we sought to confirm our observations. First, to rule out off-target effects, we amplified the DNA regions with the top potential off-target sites of the gRNAs for *D1* and no *D1* gRNA-induced off-target editing was detected (Supplementary Fig. 1J). To further exclude the possibility of off-target effects, we designed another pair of gRNAs to knock-out only exon3 of *D1* (*D1-E3-KO*), given that several species-conserved point mutations sufficient to affect the molecular function of D1 have been found in exon3[37] (Supplementary Fig. 1K). Consistently, hPGCLC efficiency was increased in *D1-E3-KO* hESCs compared to controls (Supplementary Fig. 1L, M). More importantly, we observed the increased percentage of hPGCLCs resulting from *D1-KO* in another independent hESC line[38] (Supplementary Fig. 1N). Taken together, we conclude that the increased percentage of hPGCLCs was caused by the specific deletion of *D1* from both male and female hESC lines.

To determine whether the higher percentage of hPGCLCs was due to increased cell proliferation in *D1-KO* cells, we performed EdU incorporation assays on control and *D1-KO* day 4 hPGCLC aggregates. Importantly, the percentage of EdU-positive cells was comparable between *D1-KO* and control day 4 hPGCLCs (Supplementary Fig. 1O),

https://doi.org/10.1038/s41467-025-57490-6

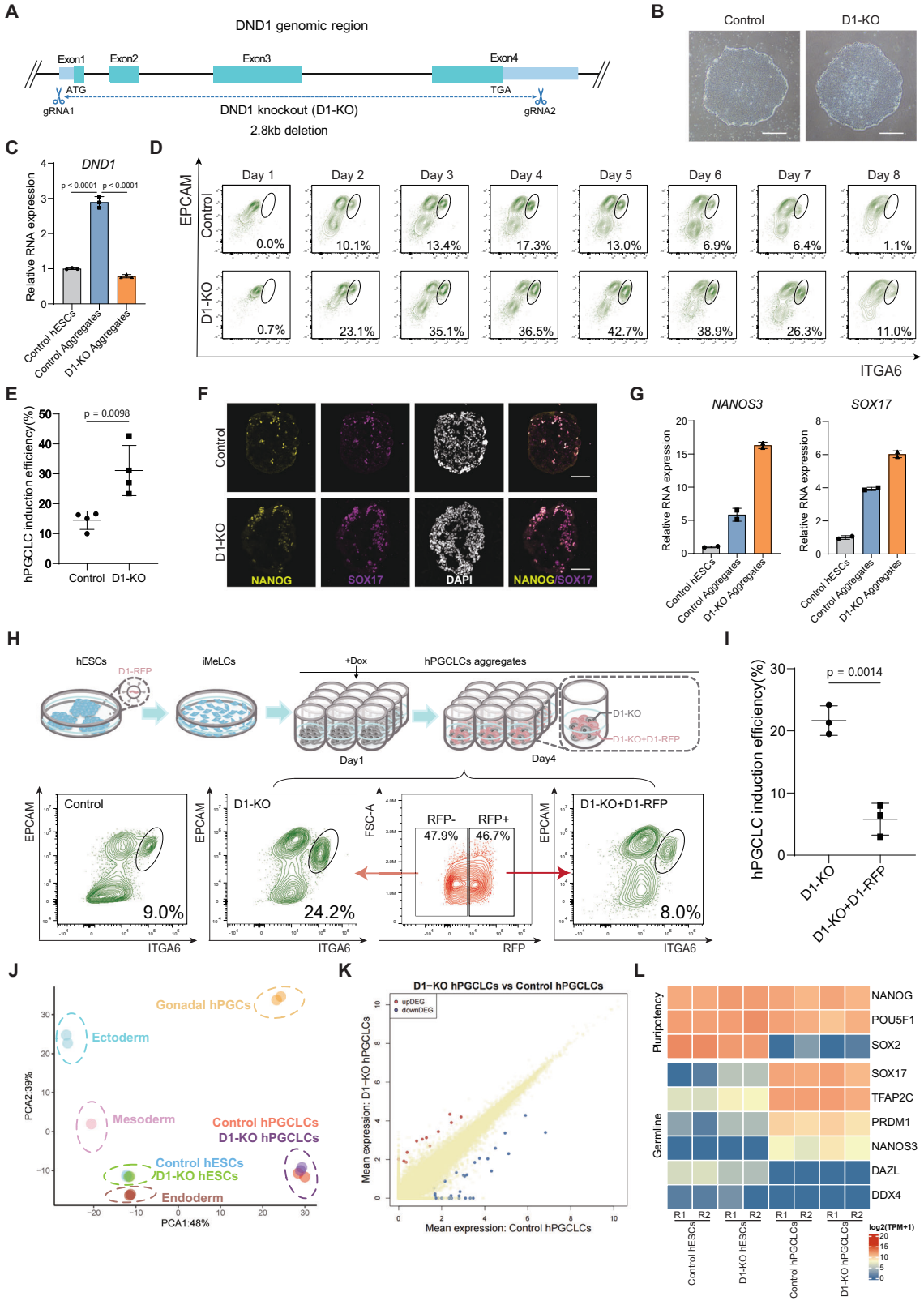

indicating that cell proliferation rates were similar. Finally, to validate our conclusion, we over-expressed *D1-RFP* in *D1-KO* aggregates. By controlling the titers of lentivirus, we achieved a mixed population of RFP-positive cells (*D1-KO* + *D1-RFP*) and RFP-negative cells (*D1-KO*) after adding Doxycycline (Dox) from day 1 of hPGCLC induction (Fig. 1H). The advantage of the strategy is that experimental and control cells are in the same wells throughout the hPGCLC induction period, thus minimizing batch variability. Over-expression of *D1-RFP* rescued the hPGCLC phenotype observed in *D1-KO* aggregates from the same transfected pools (Fig. 1H, I), confirming that the phenotype was caused by *D1* deletion in hESCs. Collectively, we conclude that D1 functions to restrict hPGCLC specification from hESCs.

To determine whether the hPGC fate was affected in *D1-KO* hESCs, we performed RNA-seq on sorted day 4 control and *D1-KO* hPGCLCs.

Fig. 1 | D1 restricts the specification of hPGCLCs from hESCs. A Illustration showing the knock-out of the genomic region of *DND1* (*D1-KO*) based on CRISPR/Cas9 strategy. **B** The morphology of control and *D1-KO* hESCs. Scale bar: 200 μm. **C** RT-qPCR showing relative RNA expression of D1 in control hESCs, control, and *D1-KO* day 4 hPGCLC aggregates. Mean with standard deviation (SD) from n = 3 experiments. Unpaired t test; two-tailed P value. Source data are provided as a Source Data file. **D** FACS analysis showing the percentages of hPGCLCs from day 1 to day 8 from control and *D1-KO* hESCs. EPCAM: Epithelial cell adhesion molecule/CD326, ITGA6: Integrin alpha-6/CD49f. **E** Statistics of hPGCLC percentages induced from control and *D1-KO* hESCs. Mean with SD from n = 4 experiments. Unpaired t test; two-tailed P value. Source data are provided as a Source Data file. **F** Immunofluorescence of NANOG (yellow) and SOX17 (magenta) in control and *D1-KO* day 4 hPGCLC aggregates. Scale bar: 40 μm. Representative images from three independent experiments. **G** RT-qPCR showing relative expression levels of *NANOS3* and *SOX17* in control hESCs, control and *D1-KO* day 4 hPGCLC aggregates. Source data are provided as a Source Data file. **H** Top: Schematic illustration showing the rescue strategy in hPGCLC induction. Bottom: FACS analysis showing the percentages of hPGCLCs using control and *D1-KO* + *D1-RFP* hESCs. iMeLCs: incipient mesoderm/primitive streak-like cells. **I** Statistics of hPGCLC percentages induced from *D1-KO* (RFP negative) and *D1-KO* + *D1-RFP* (RFP positive) day 4 hPGCLCs. Mean with SD from n = 3 experiments. Unpaired t test; two-tailed P value. Source data are provided as a Source Data file. **J** PCA plot showing the transcriptomes of control and *D1-KO* hESCs, control and *D1-KO* day 4 hPGCLCs, gonadal hPGCs[8], and hESC-derived endoderm, mesoderm, and ectoderm. **K** Plot showing the DEGs of control and *D1-KO* day 4 hPGCLCs. **L** Heatmap showing the expression of pluripotency and PGC marker genes in control and *D1-KO* hESCs, sorted control, and *D1-KO* day 4 hPGCLCs. R replicate. See also Supplementary Fig. 1.

Intriguingly, *D1-KO* hPGCLCs clustered with control hPGCLCs and separated from gonadal hPGCs and hESC-derived endoderm, mesoderm, and ectoderm in the principal component analysis (PCA) plot (Fig. 1J), suggesting that hPGCLC fate was probably not altered in *D1-KO*. 12 up-regulated DEGs and 31 down-regulated DEGs were identified between *D1-KO* and control hPGCLCs (Fig. 1K; Supplementary Data 1). Additionally, the expression of hPGC genes was comparable between *D1-KO* and control hPGCLCs (Fig. 1L), further confirming that hPGCLC fate was not changed. Altogether, these results demonstrate that D1 restricts the entry of hPGCLC fate induced from hESCs.

D1 functions with NANOS3 to suppress the induction of hPGCLCs from hESCs

D1 is a typical RBP with two RNA recognition motifs (Supplementary Fig. 2A). RBPs tend to regulate bound target RNAs via interactions with other RBPs and non-RBPs in the form of ribonucleoprotein (RNP) complexes[31]. Therefore, we sought to identify the interacting partners of D1 in germ cell development. A D1-interactome was previously captured in HEK293T cells via co-IP-MS[28]. We overlapped these D1-interacting proteins with hPGCLC-specific genes from our previous study[39,40]. Interestingly, only NANOS3 (N3) was identified (Fig. 2A). N3 belongs to the NANOS family that regulates germ cell development in various organisms[20,32,41]. Though N3 has served as one of the key PGC markers for decades due to its PGC-specific expression pattern[19,20,39] (Supplementary Fig. 2B, C), the function of N3 in the regulation of hPGCLC development is incompletely characterized. We verified the physical interaction between D1 and N3 by co-IP in hESCs with over-expression of D1 and N3 (Fig. 2B), and this interaction was RNA-independent (Supplementary Fig. 2D).

To determine whether N3 is involved in the regulation of hPGCLCs induced from hESCs, we first deleted the entire genomic region of *N3* (Supplementary Fig. 2E). The *N3* knock-out (*N3-KO*) hESCs were morphologically and karyotypically normal (Fig. 2C; Supplementary Fig. 2F), positive for the pluripotency marker SSEA4 by flow cytometry (Supplementary Fig. 2G), and expressed pluripotency genes *NANOG, SOX2, PRDM14*, and OCT4 by qPCR and immunofluorescence (Supplementary Fig. 2H, I). These observations suggest that N3 is not essential for the maintenance of hESCs. Next, we tested the differentiation capacity of *N3-KO* cells by forming embryoid bodies. Expectedly, the pluripotency gene (*POU5F1*) was decreased, while endoderm (*GATA4, GATA6*), mesoderm (*T, EVX1, MSX2*), and ectoderm (*PAX6*) genes were up-regulated (Supplementary Fig. 2J), suggesting that the N3 is not essential for the differentiation of hESCs. This is consistent with the observation that *N3* is a germ cell-specific gene in vivo[7,8,39]. Furthermore, the percentage of apoptotic cells was comparable between *N3-KO* and control hESCs (Supplementary Fig. 2K), and the proliferation rate was comparable between *N3-KO* and control hESCs, as determined by the EdU incorporation assay (Supplementary Fig. 2L). We also performed RNA-seq on *N3-KO* hESCs and identified 337 up-regulated and 146 down-regulated DEGs (Supplementary Fig. 2M; Supplementary Data 1). GO term analysis indicated the upregulation of cellular cation homeostasis and divalent inorganic cation homeostasis-related biological processes in *N3-KO* hESCs (Supplementary Fig. 2M; Supplementary Data 1). Taken together, we conclude that N3 is not essential for the maintenance and pluripotency of hESCs.

Next, we sought to determine whether N3 is involved in the regulation of hPGCLCs induced from hESCs. First, we examined the expression of *N3* in day 4 hPGCLC aggregates. As expected, *N3* was up-regulated in control but not in *N3-KO* cells (Fig. 2D), confirming the deletion of *N3*. Interestingly, the percentage of hPGCLCs increased in day 4 aggregates induced from *N3-KO* compared with control hESCs (Fig. 2E, F). To confirm this phenotype, we examined the expression of hPGCLC markers OCT4, SOX17, and PRDM1 in control and *N3-KO* day 4 hPGCLC aggregates. Consistently, more OCT4, SOX17, and PRDM1 triple-positive hPGCLCs were observed in *N3-KO* hPGCLC aggregates compared with the control group (Fig. 2G). This was also confirmed by qPCR determination of hPGC-related genes (Fig. 2H). We also observed the increased percentages of hPGCLCs in *N3-KO* generated in another hESC line[38] (Supplementary Fig. 2N), ruling out the possibility that the phenotype was cell-line dependent. Furthermore, the proliferation rate was similar between *N3-KO* and control hPGCLCs, as determined by the EdU incorporation assay (Supplementary Fig. 2O). To confirm that the observed phenotype was caused by the deletion of *N3*, we over-expressed *N3-GFP* in *N3-KO* aggregates for hPGCLC induction. Importantly, the increased percentage of hPGCLCs in *N3-KO* cells was rescued by over-expression of *N3-GFP* (Fig. 2I, J). Together, these data indicate that N3, like its interacting RBP D1, functions to restrict the specification of hPGCLCs from hESCs.

To determine the potential cell fate changes at the transcriptomic level, we performed RNA-seq on day 4 *N3-KO* and control hPGCLCs sorted using surface markers ITGA6 and EPCAM. *N3-KO* hPGCLCs clustered with control and *D1-KO* hPGCLCs in PCA plot (Fig. 2K), and 10 up-regulated DEGs and 20 down-regulated DEGs were identified in *N3-KO* hPGCLCs compared with control hPGCLCs (Fig. 2L; Supplementary Data 1). Furthermore, the expression of hPGC-related genes was comparable between *N3-KO* and control hPGCLCs (Fig. 2M). suggesting that the hPGCLC fate was not affected in *N3-KO* cells. Altogether, these data indicate that N3 also functions to restrict germline entry during the specification of hPGCLCs from hESCs, likely via cooperation with D1.

D1 and N3 cooperatively restrict the specification of hPGCLCs from hESCs

To further explore how the D1-N3 complex restricts the induction of hPGCLCs from hESCs, we generated double knock-out of *D1* and *N3* (*D1-N3-dKO*) hESCs. The double deletion of *D1* and *N3* was confirmed by qPCR analysis of *D1* and *N3* expression in *D1-N3-dKO* and control day 4 hPGCLC aggregates (Fig. 3A). As hypothesized, the percentage of induced hPGCLCs increased from *D1-N3-dKO* hESCs relative to control, consistent with observations from single knockouts of *D1* and *N3*

https://doi.org/10.1038/s41467-025-57490-6

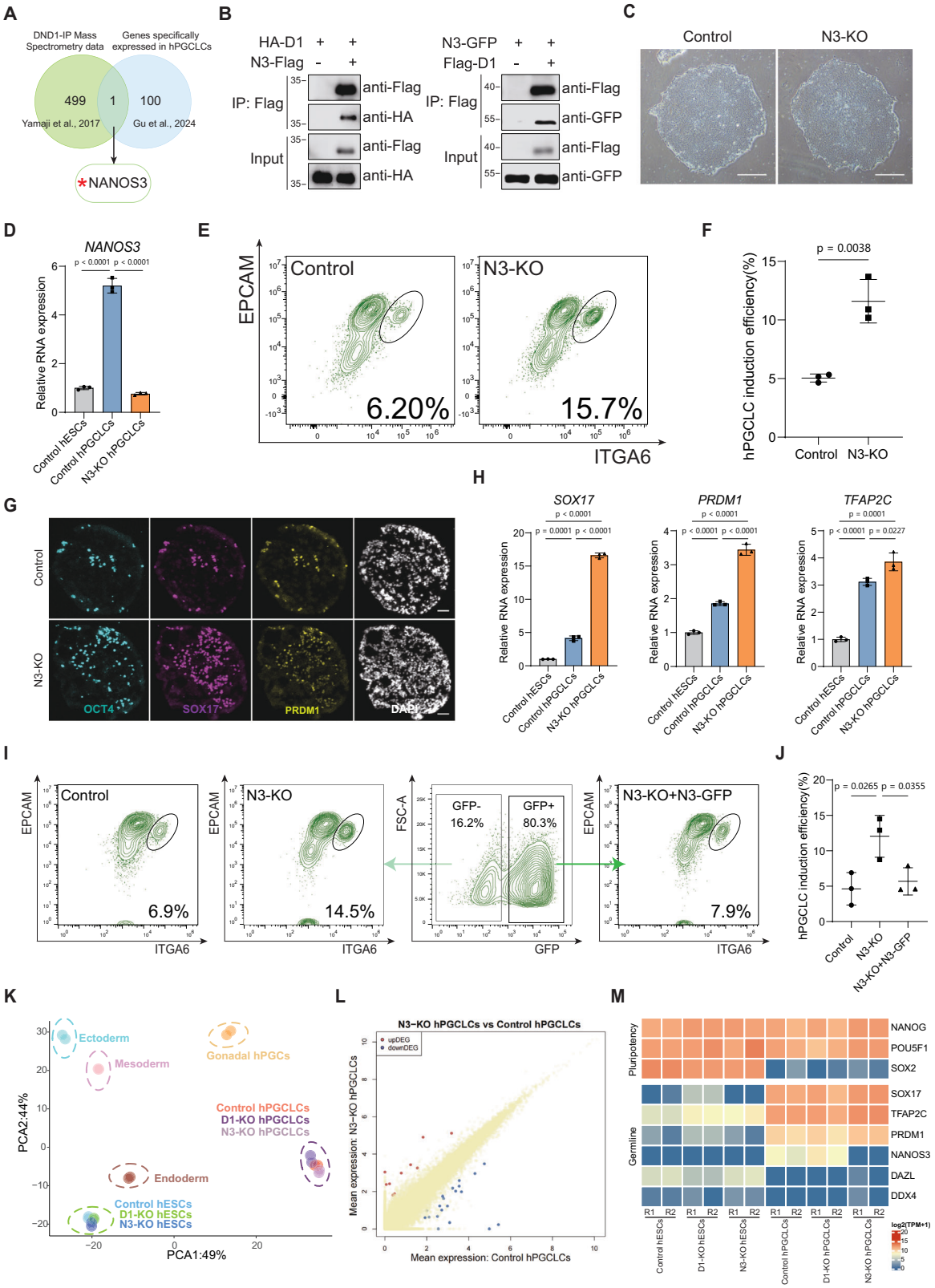

(Fig. 3B, C; Supplementary Fig. 3A), further supporting that D1 and N3 function together to restrict hPGCLC induction. Consistently, more OCT4-positive hPGCLCs were detected in day 4 hPGCLC aggregates induced from *D1-N3-dKO* hESCs compared to control by immunofluorescence (Supplementary Fig. 3B). To further characterize the functions of D1 and N3 in hPGCLC induction, we performed RNA-seq on *D1-N3-dKO* day 4 hPGCLCs sorted using surface markers ITGA6 and EPCAM. *D1-N3-dKO*, *D1-KO*, *N3-KO*, and control hPGCLCs clustered together in a PCA plot (Fig. 3D), and 34 up-regulated DEGs and 60 down-regulated DEGs were identified in *D1-N3-dKO* hPGCLCs compared to control day 4 hPGCLCs (Fig. 3E; Supplementary Data 1). Moreover, the expression of germ cell markers was comparable among *D1-N3-dKO*, *D1-KO*, *N3-KO*, and control hPGCLCs (Fig. 3F; Supplementary Fig. 3C), further supporting that D1 and N3 function as a complex.

Fig. 2 | N3 suppresses the induction of hPGCLCs from hESCs. A Venn diagram showing the overlap of D1-interacting proteins[28] and hPGCLC-specific genes[40]. **B** Reciprocal co-immunoprecipitation showing the physical interaction of D1 and N3 in hESCs. Representative images from three independent experiments. Source data are provided as a Source Data file. **C** The morphology of control and *N3-KO* hESCs. Scale bar: 200 µm. **D** RT-qPCR showing relative expression levels of *N3* in control hESCs, control and *N3-KO* day 4 hPGCLC aggregates. Mean with SD from n = 3 experiments. Unpaired t test; two-tailed P value. Source data are provided as a Source Data file. **E** Flow cytometry showing the percentages of day 4 hPGCLCs induced from control and *N3-KO* hESCs. **F** Statistics of hPGCLC percentages from control and *N3-KO* hESCs. Mean with SD from n = 3 experiments. Unpaired t test; two-tailed P value. Source data are provided as a Source Data file. **G** Immunofluorescence of OCT4 (cyan), SOX17 (magenta) and PRDM1 (yellow) in control and *N3-KO* day 4 hPGCLC cryosection. Scale bar: 20 µm. Representative images from three independent experiments. **H** RT-qPCR showing relative expression levels of *SOX17, PRDM1 and TFAP2C* in control hESCs, control and *N3-KO* day 4 hPGCLC aggregates. Mean with SD from n = 3 experiments. Unpaired t test; two-tailed P value. Source data are provided as a Source Data file. **I** Flow cytometry showing the percentages of hPGCLCs induced from control and *N3-KO* + *N3-GFP* hESCs. **J** Statistics of hPGCLC percentages from control, *N3-KO* (GFP negative) and *N3-KO* + *N3-GFP* (GFP positive) day 4 hPGCLCs. Mean with SD from n = 3 experiments. Unpaired t test; two-tailed P value. Source data are provided as a Source Data file. **K** PCA plot showing the transcriptomes of control, *D1-KO*, *N3-KO* hESCs, and sorted control, *D1-KO*, *N3-KO* day 4 hPGCLCs, gonadal hPGCs[8], and hESC-derived endoderm, mesoderm, and ectoderm. **L** Plot showing the DEGs of control and *N3-KO* day 4 hPGCLCs. **M** Heatmap showing the expression of pluripotency and PGC marker genes in control, *D1-KO*, *N3-KO* hESCs, and sorted control, *D1-KO*, *N3-KO* day 4 hPGCLCs. See also Supplementary Fig. 2.

Taken together, these results suggest that the D1-N3 complex functions together to suppress the specification of germ cell fate.

To further investigate the repressive roles of the D1-N3 complex in hPGCLC induction, we examined whether over-expression of D1 and N3, separately or simultaneously, would impair the specification of hPGCLCs induced from hESCs. We first over-expressed RFP-tagged D1 (*D1-RFP*) in hESCs using the same method as over-expressing D1-RFP to rescue *D1-KO* phenotype (Fig. 1H). By separating RFP positive (D1-OE) and RFP negative (control) cells, we found that the hPGCLC percentage decreased dramatically in D1-OE compared to control (Fig. 3G, H), consistent with our observations that D1 restricts the specification of hPGCLCs from hESCs (Fig. 1). We then performed immunofluorescence on the day 4 hPGCLC aggregates. NANOG is specifically expressed in hPGCLCs in day 4 aggregates. Importantly, most NANOG-positive cells are D1-RFP-negative and vice versa (Supplementary Fig. 3D), further supporting that D1 restricts hPGCLC induction. Next, we applied the same strategy to over-express N3-GFP. Similarly, over-expression of N3-GFP (N3-OE) led to a decreased percentage of hPGCLCs (Fig. 3I, J). Consistently, most *N3-OE* cells (GFP-positive) were negative for the hPGCLC marker OCT4, and most OCT4-positive cells were negative for GFP (N3-OE) in day 4 aggregates (Supplementary Fig. 3E). These results further indicate that N3 restricts the specification of hPGCLCs from hESCs. We then over-expressed both D1 and N3 in hESCs for hPGCLC induction. In this set of experiments, we obtained the following genotypes simultaneously, (1) control, (2) *N3-OE*, (3) *D1-OE*, and (4) *D1-N3-dOE*. Consistently, over-expression of N3 or D1 decreased the percentages of hPGCLCs, with D1 having a more severe effect, similar to D1-N3-dOE (Fig. 3K, L; Supplementary Fig. 3F). Importantly, we verified the phenotype of *N3-OE* and *D1-OE* in another hESC line for hPGCLC induction (Supplementary Fig. 3G, H). Altogether, we conclude that D1 and N3 function cooperatively to restrict the entry of germ cell fate induced from hESCs.

Identification of the mRNAs bound by D1 and N3 in hPGCLCs

Given that D1 and N3 are RNA-binding proteins, we aimed to identify the D1-N3 target mRNAs that are likely regulated to elicit control of hPGCLC specification. We employed the inducible TRIBE (iTRIBE) strategy[42,43] (Fig. 4A). First, we generated hESC lines with Doxycycline (Dox)-inducible expression of D1 or N3 fused to the V5-tagged catalytic domain of ADAR (*tetON-D1-ADAR* and *tetON-N3-ADAR*, respectively). To minimize potential side effects from over-expression of D1 or N3 and the adenosine-to-inosine (A-to-I) conversion on target mRNAs by ADAR, we strictly administered Dox to ensure D1-ADAR/N3-ADAR expression only during the hPGCLC stage. The expression of D1-ADAR and N3-ADAR was confirmed by anti-V5 western blot (Supplementary Fig. 4A). Next, we performed RNA-seq on sorted day 4 hPGCLCs induced from hESCs over-expressing D1-ADAR and N3-ADAR separately. As expected, *D1-ADAR* and *N3-ADAR* were expressed in the hPGCLCs derived from the respective hESC lines (Supplementary Fig. 4B). Transcriptomic analysis showed that *D1-ADAR* and *N3-ADAR* hPGCLCs clustered with control, *D1-KO*, *N3-KO*, and *D1-N3-dKO* hPGCLCs in a PCA plot (Supplementary Fig. 4C). Additionally, there were 70 up-regulated and 76 down-regulated DEGs in *D1-ADAR* hPGCLCs, and 55 up-regulated and 92 down-regulated DEGs in *N3-ADAR* hPGCLCs, compared to control hPGCLCs (Supplementary Fig. 4D and S4E; Supplementary Data 1), indicating that over-expression of D1-ADAR or N3-ADAR did not alter the germ cell fate of hPGCLCs. Consistently, the expression levels of PGC markers were comparable among *D1-ADAR*, *N3-ADAR*, and control hPGCLCs (Supplementary Fig. 4F).

The binding of D1-ADAR and N3-ADAR to mRNAs was identified through ADAR-mediated A-to-I editing, which manifests as A-to-G conversion in sequencing data. The editing events we detected were predominantly enriched in 3'UTR and coding sequences (CDS) and peaking around stop codons for both D1 and N3 (Fig. 4B). We identified 2,876 and 3,230 editing sites for D1-ADAR and N3-ADAR, respectively (Fig. 4C; Supplementary Data 2). GO term analyses indicated that the D1-bound mRNAs and N3-bound mRNAs in hPGCLCs were enriched for terms such as in utero embryonic development and RNA splicing (Supplementary Fig. 4G, H; Supplementary Data 3). Notably, some mRNAs were detected as bound by both D1 and N3 (such as *NANOG*), some by D1 (such as *RGS3*), and some by N3 (such as *CEBPD*) (Fig. 4D).

Given that D1 and N3 interact with each other physically (Fig. 2B) and the similar binding motifs in hPGCLCs based on our iTRIBE data (Fig. 4E), we next analyzed the target mRNAs bound by both D1 and N3. We identified 746 mRNAs bound by both D1 and N3 (Fig. 4F), and GO analysis revealed that the encoding genes were enriched for terms such as Wnt signaling pathway (Fig. 4G; Supplementary Data 3), which has been reported to regulate the development of human germ cells[44,45]. We also analyzed the mRNAs bound by D1 or N3 separately. The genes encoding D1-only-bound mRNAs were enriched for terms such as proteasome-mediated ubiquitin-dependent protein catabolic processes, *in utero* embryonic development and cell growth; while the genes encoding N3-only-bound mRNAs were enriched for terms including RNA splicing and regulation of mRNA metabolic process (Supplementary Fig. 4I, J; Supplementary Data 3).

To determine whether D1/N3-binding and/or expression affects their target mRNAs, we analyzed the expression level of the 746 genes bound by both D1 and N3 in control, *D1-ADAR*, *D1-KO*, *N3-ADAR*, and *N3-KO* hPGCLCs. The expression levels of these 746 genes were comparable among these groups of hPGCLCs (Fig. 4H; Supplementary Fig. 4K), suggesting that the D1-N3 complex may be involved in translational regulation. In conclusion, our results reveal that the D1-N3 complex binds to mRNAs in hPGCLCs that are related to germ cell development.

D1 recruits N3 to bind to hPGCLC-related target mRNAs

The RNA editing-based techniques allow the identification of target mRNAs co-bound by two RBPs. We leveraged A to I (G) conversion by ADAR for one RBP and C to T conversion by rat APOBEC1 (rAPO)

https://doi.org/10.1038/s41467-025-57490-6

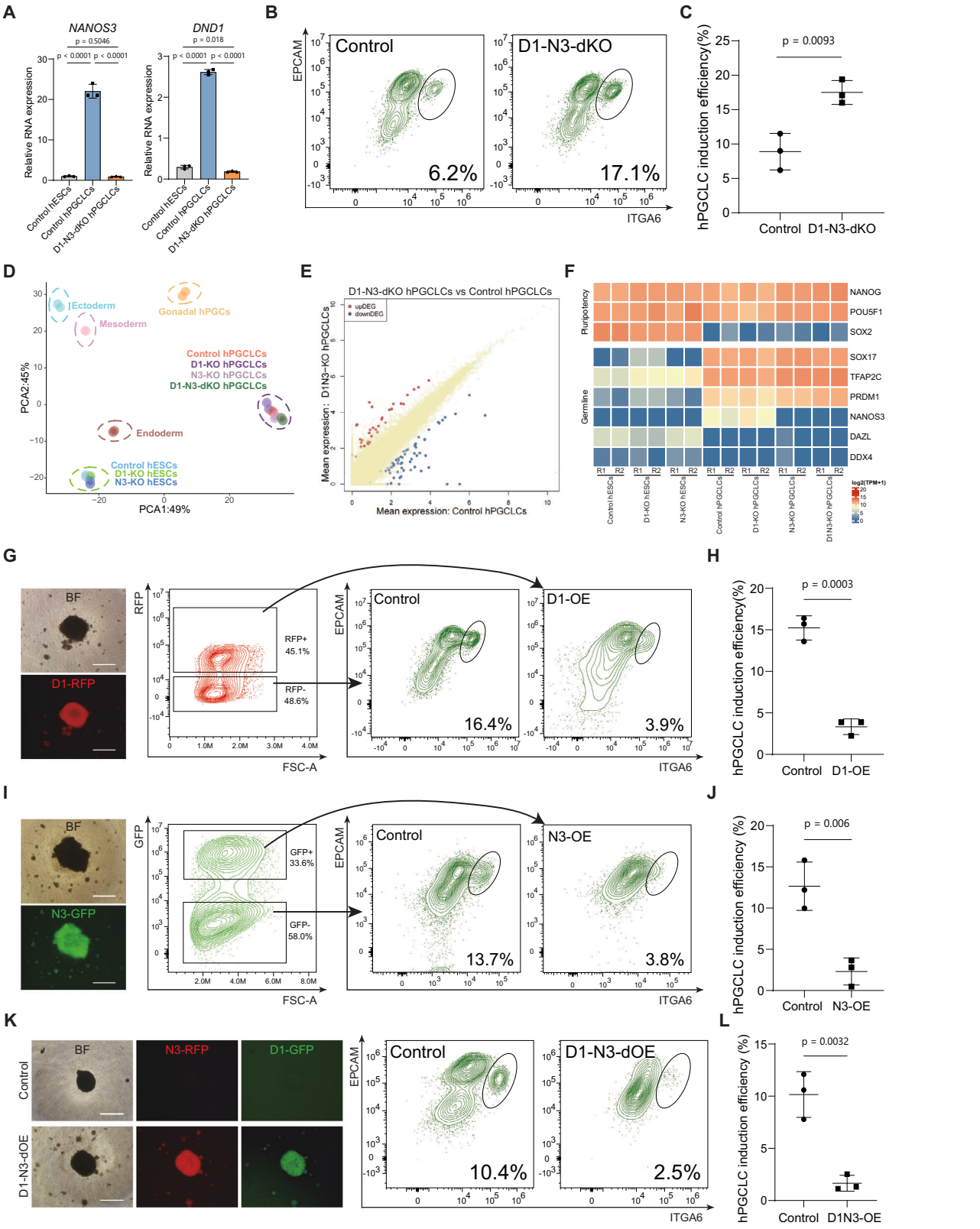

(TRIBE-STAMP)[46–48] (Fig. 5A). We then aimed to analyze the mRNAs co-bound by D1 and N3 in hESCs by characterizing the functional relationship between these RBPs. Due to the impairment of hPGCLC induction by simultaneous over-expression of D1 and N3 in hESCs (Fig. 3K, L; Supplementary Fig. 3F), we over-expressed separately D1-ADAR, N3-ADAR, or D1-rAPO+N3-ADAR in hESCs. This strategy allowed us to capture mRNAs bound by D1 alone (Corresponding to *N3-KO* hPGCLCs), bound by N3 alone (Corresponding to *D1-KO* hPGCLCs), or co-bound by D1 and N3 (Corresponding to control hPGCLCs with both D1 and N3), respectively, given that hPGCLCs show high similarity to hESCs at both transcriptional and chromatin levels[13].

We first evaluated the transcriptomes of hESCs with over-expression of D1-ADAR, N3-ADAR, and D1-rAPO+N3-ADAR to confirm that cell fate was not altered due to the over-expression of the

Fig. 3 | D1 and N3 cooperatively restrict the induction of hPGCLCs from hESCs. **A** RT-qPCR showing relative expression levels of *D1* and *N3* in control hESCs, control and *D1-N3-dKO* day 4 hPGCLCs. Mean with SD from n = 3 experiments. Unpaired t test; two-tailed P value. Source data are provided as a Source Data file. **B** FACS analysis showing the percentages of control and *D1-N3-dKO* day 4 hPGCLCs. **C** Statistics of hPGCLC percentages from control and *D1-N3-dKO* hESCs. Mean with SD from n = 3 experiments. Unpaired t test; two-tailed P value. Source data are provided as a Source Data file. **D** PCA plot showing the transcriptomes of control, *D1-KO*, *N3-KO*, *D1-N3-dKO* hESCs, and sorted control, *D1-KO*, *N3-KO*, *D1-N3-dKO* day 4 hPGCLCs, gonadal hPGCs[8], and hESC-derived endoderm, mesoderm, and ectoderm. **E** Plot showing the DEGs of control and *D1-N3-dKO* day 4 hPGCLCs. **F** Heatmap showing the expression of pluripotency and PGC marker genes in control, *D1-KO*, *N3-KO* hESCs, and sorted control, *D1-KO*, *N3-KO*, *D1-N3-dKO* day 4 hPGCLCs. **G** FACS analysis showing the percentages of control (RFP negative) and D1-OE (RFP positive) day 4 hPGCLCs. Scale bar: 80 µm. **H** Statistics of hPGCLC percentages from control and D1-OE hESCs. Mean with SD from n = 3 experiments. Unpaired t test; two-tailed P value. Source data are provided as a Source Data file. **I** FACS analysis showing the percentages of control (GFP negative) and N3-OE (GFP positive) day 4 hPGCLCs. Scale bar: 80 µm. **J** Statistics of hPGCLC percentages from control and N3-OE hESCs. Mean with SD from n = 3 experiments. Unpaired t test; two-tailed P value. Source data are provided as a Source Data file. **K** FACS analysis showing the percentages of control and D1-N3-dOE day 4 hPGCLCs. Scale bar: 80 µm. **L** Statistics of hPGCLC percentages from control and D1-N3-dOE hESCs. Mean with SD from n = 3 experiments. Unpaired t test; two-tailed P value. Source data are provided as a Source Data file. See also Supplementary Fig. 3.

corresponding genes. Importantly, these overexpressing hESC lines were clustered with corresponding control, *D1-KO*, and *N3-KO* cells but were distinct from other germ layer cells in PCA plots (Supplementary Fig. 5A), indicating that the over-expression of ADAR/rAPO-tagged D1/N3 did not lead to detectable cell fate alteration. Consistently, compared to control hESCs, 159 up- and 105 down-regulated DEGs were identified for *D1-ADAR* hESCs, 541 up- and 228 down-regulated DEGs were identified for *N3-ADAR* hESCs, and 250 up- and 60 down-regulated DEGs were identified for *D1-rAPO + N3-ADAR* hESCs (Supplementary Fig. 5B–D; Supplementary Data 1). GO term analysis indicated upregulation of nervous system development, negative regulation of cell development-related biological processes, and downregulation of ossification and bone mineralization regulation processes in *D1-ADAR* hESCs (Supplementary Fig. 5B; Supplementary Data 1). For *N3-ADAR* hESCs, the up-regulated DEGs were associated with pattern specification, forebrain development, while down-regulated DEGs were associated with regulation of endopeptidase activity and steroid metabolic process (Supplementary Fig. 5C; Supplementary Data 1). For *D1-rAPO + N3-ADAR* hESCs, pattern specification process and ameboidal-type cell migration were the top two significant up-regulated biological processes (Supplementary Fig. 5D; Supplementary Data 1).

We then evaluated co-edited mRNAs by D1-rAPO (C to T) and N3-ADAR (A to G) in hESCs by comparing to the TRIBE-STAMP of YTHDF1/2/3[48]. Approximately 19.0% (353 mRNAs) of all edited reads were co-edited, compared about 19.3% (171 mRNAs) to 80.5% (3268 mRNAs) from the TRIBE-STAMP of YTHDF1/2/3[48] (Fig. 5B, C; Supplementary Data 4), indicating that we could analyze the target mRNAs bound by D1 and N3 simultaneously for further analysis. These observations prompted us to analyze the inter-dependency of RNA-binding between D1 and N3.

First, we identified the editing sites by D1-ADAR (D1-alone), N3-ADAR (N3-alone), and D1-rAPO+N3-ADAR (D1 + N3) in hESCs. There were 27,218 editing sites for D1 only and 5259 editing sites for *N3-alone*, 4645 editing sites for D1-binding and 20,468 editing sites for N3-binding in *D1 + N3* (Fig. 5D; Supplementary Data 4). Most of these editing sites were located in the 3'UTR (Supplementary Fig. 5E), typical regulatory regions bound by RBPs[49]. Next, we further analyzed whether D1 promotes N3 binding to their target mRNAs by comparing N3 target mRNAs in hPGCLCs and hESCs, as N3 (and D1) is normally expressed in hPGCLCs but not hESCs. We found that only 24.3% (456 genes) of hPGCLC-N3-mRNAs (the mRNAs bound by N3 in hPGCLCs) were captured in *N3-alone* hESCs. Strikingly, 61.4% (1130 genes) of hPGCLC-N3-mRNAs were captured by N3 in *D1 + N3* hESCs (Fig. 5E), supporting the conclusion that D1 promotes N3 binding to hPGCLC-related target mRNAs.

To exclude the possibility that increased capture of hPGCLC-N3-mRNAs in hESCs bound by N3 after D1 over-expression was due to transcriptome changes, we compared the 456 overlapping mRNA targets between N3-ADAR hPGCLCs and *N3-alone* hESCs, and the 1,130 overlapping mRNA targets between N3-ADAR hPGCLCs and *D1 + N3* hESCs. We focused on 722 mRNA targets that were bound by N3 in hESCs only in the presence of D1 (Supplementary Fig. 5F). The expression levels of these 722 mRNA targets were similar between *N3-alone* and *D1 + N3* groups, indicating that N3 binding to these mRNAs was determined by D1 presence, not expression levels (Supplementary Fig. 5G, H). Consistently, *N3-alone* hESCs exhibited binding motif preference that is distinct from those in hPGCLCs (Fig. 5G, rightmost), while over-expression of *D1* in *N3-alone* hESCs shifted the enriched binding motifs of N3 towards those of D1 and N3 in hPGCLCs (Fig. 5F). Taken together, based on the above results, our results suggest that D1 alters the specificity of N3 from being N3-direct targets to D1-dependent targets which are hPGCLC-related mRNAs (Fig. 5G).

Identification of *SOX4* as a critical target gene for D1-N3 in regulating the induction of hPGCLCs

Next, we sought to identify the key target mRNAs regulated by the D1-N3 RBP complex in hESC to hPGCLC induction. We leveraged the over-expression of D1-rAPO and N3-ADAR in hESCs for capturing the target mRNAs bound by D1-only, N3-only, and D1-N3 complex (Fig. 5), and we identified 187 mRNA targets that were putatively co-bound by D1 and N3 in both hESCs and hPGCLCs, representing potential mRNAs bound by D1-N3 complex in regulating hPGCLC induction (Supplementary Fig. 6A). Previous comparisons showed that N3's binding to hPGCLC-related mRNA targets is dependent on the presence of D1 (Fig. 5). Therefore, we hypothesize that among these 187 mRNA targets, those with the most significant change in N3 binding strength, from the absence to the presence of D1, are likely crucial downstream effectors of the D1-N3 complex. Next, we quantified the N3 binding strength by RNA editing scores[48] and identified *SOX4* as the strongest candidate (Fig. 6A). Recently, we have discovered SOX4 as a potentially key transcription factor for hPGCLC development[40]. Notably, *SOX4* is expressed throughout the germline trajectory from hESCs to hPGCLCs[40] (Supplementary Fig. 6B). To further confirm the involvement of SOX4 in hPGCLC induction, we designed a CRISPRi-based knock-down (KD) approach for *SOX4* and verified that the percentage of hPGCLCs significantly decreased in *SOX4-KD* cells compared to controls (Fig. 6B, C; Supplementary Fig. 6C). To functionally test whether the D1-N3 complex acts through SOX4 in regulating hPGCLC development, we knocked down *SOX4* in both *D1-KO* and *N3-KO* hESCs for hPGCLC induction. Notably, knock-down of *SOX4* suppressed both *D1-KO* and *N3-KO* phenotype (Fig. 6D; Supplementary Fig. 6D), consistent with our hypothesis that D1-N3 complex functions through *SOX4* in hESC to hPGCLC induction.

We then examined the expression level of *SOX4* based on RNA-seq analysis of control, *D1-KO*, *N3-KO*, *D1-OE*, *N3-OE*, and *D1-N3-dOE* hESCs, as well as control, *D1-KO*, *N3-KO*, *D1-N3-dKO*, *D1-OE*, and *N3-OE* hPGCLCs. Consistently, the mRNA levels of *SOX4* were not changed in *D1-KO*, *N3-KO*, *D1-OE*, or *N3-OE* groups (Supplementary Fig. 6E). These observations strongly indicate that D1-N3 complex may regulate the translational level of *SOX4* rather than transcriptional level. To test

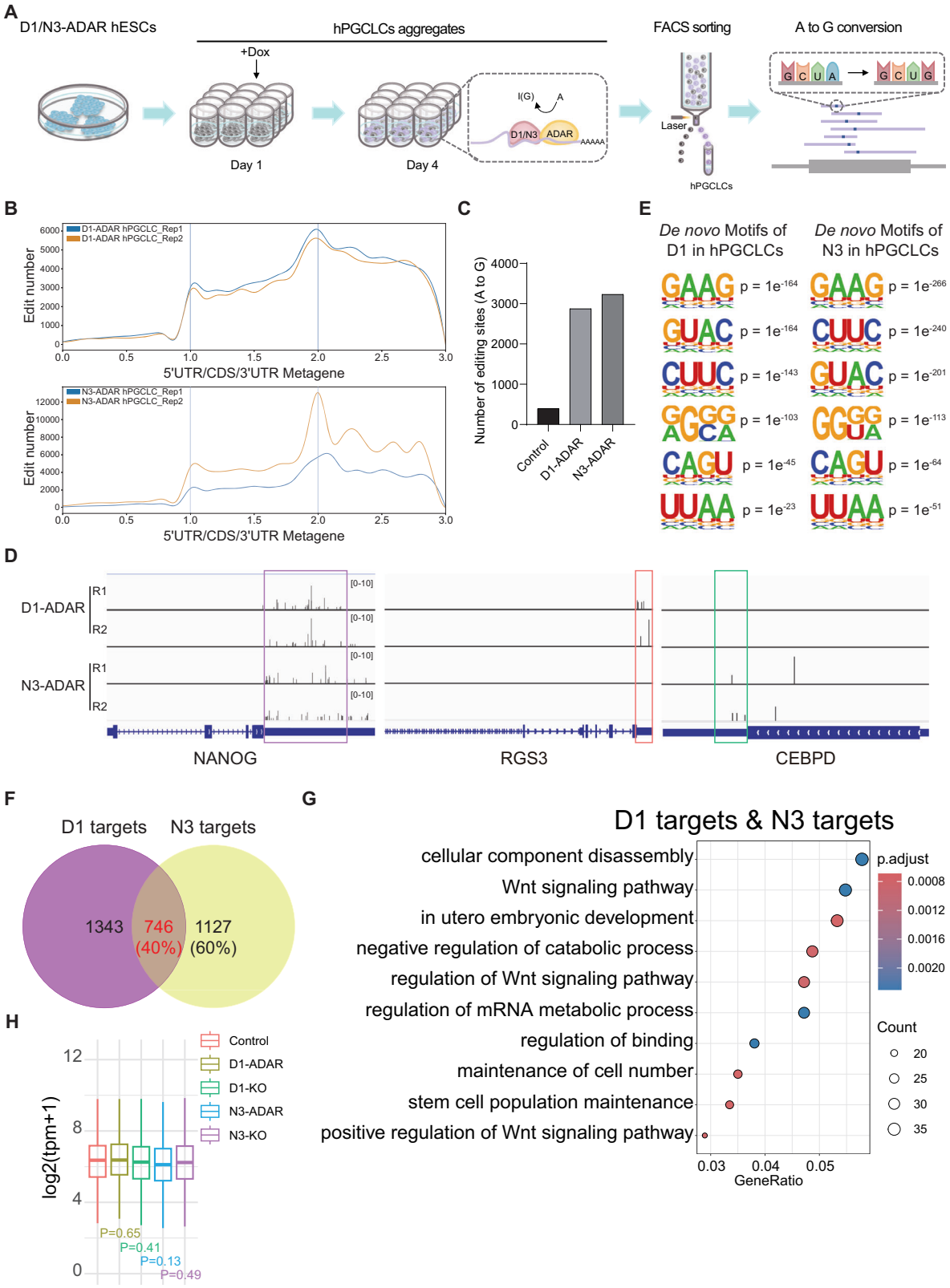

this possibility, we performed immunofluorescence using antibodies against SOX4 in control, *D1-KO*, *N3-KO*, and *D1-N3-dKO* hPGCLC aggregates. To be noted, SOX4 protein levels were significantly increased in *D1-KO*, *N3-KO*, and *D1-N3-dKO* hPGCLCs labeled by OCT4, whereas OCT4 protein levels were almost unchanged (Fig. 6E). To further confirm this observation, we took advantage of over-expressing N3 alone, D1 alone, D1-N3-together in hESCs and discovered that either N3- or D1-alone had no dramatic effect on the protein level of SOX4, however, when D1 and N3 were over-expressed simultaneously, the protein level of SOX4 was dramatically decreased while the mRNA level of *SOX4* was not changed (Fig. 6F, G). Taken together, these data reveal that the D1-N3 complex regulates the translational level of *SOX4* for restricting hPGCLC induction from hESCs.

Fig. 4 | Identification of the mRNAs bound by D1 and N3 in hPGCLCs. **A** Schematic illustration of the iTRIBE strategy for capturing the mRNAs bound by D1 and N3 in hPGCLCs. **B** Distribution of the editing sites of D1-ADAR (top) and N3-ADAR (bottom) in day 4 hPGCLCs. **C** Bar graph showing the number of editing sites (**A**–**G**) detected in control, *D1-ADAR* and *N3-ADAR* day 4 hPGCLCs. **D** Tracks showing the mRNAs bound by both D1 and N3 (left), D1 only (middle), and N3 only (right). **E** Top enriched de novo motifs identified within 100 bp upstream and downstream of the D1 and N3 editing sites. A one-sided hypergeometric test was employed to determine whether particular motifs are significantly overrepresented in the target set compared to background regions. **F** Venn diagram showing the overlap of D1 target mRNAs and N3 target mRNAs. Purple: D1 target mRNAs, Yellow: N3 target mRNAs. **G** GO term analysis of the 746 mRNA targets bound by both D1 and N3 in (**F**). To account for multiple hypothesis testing, p values were adjusted using the Benjamini-Hochberg method. Multiple comparisons are adjusted using FDR (q-value) and q value Cutoff = 0.2 to control the false discovery rate. **H** Box plots showing the transcript abundance of control, *D1-ADAR*, *D1-KO*, *N3-ADAR*, and *N3-KO* hPGCLCs for the mRNA targets bound by both D1 and N3 in (**F**). Statistical significance between groups was calculated using two-tailed unpaired t-tests, comparing experimental groups to the control groups. Data are shown as Mean with SD. The minimum and maximum values were defined as the lowest and highest data points within 1.5 times the interquartile range (IQR) from the first and third quartiles, respectively. The center of the box represents the median, and the upper and lower boundaries of the box correspond to the first and third quartiles (25th and 75th percentiles). The whiskers extend to the most extreme data points within 1.5 IQR of the quartiles, and data points beyond this range are plotted as outliers. See also Supplementary Fig. 4.

D1-N3 complex represses the translation of *SOX4* mRNAs in P-bodies

To explore how the D1-N3 complex regulates the protein level of SOX4, we analyzed the sub-cellular localization of D1 and N3. When over-expressed in hESCs, D1 protein was detected in both the nucleus and cytoplasm (Fig. 7A). Given that translational regulation occurs in the cytoplasm[50–52], we focused on the cytoplasmic D1. The presence of D1 protein puncta in the cytoplasm suggests that D1 may localize to processing bodies (P-bodies). Indeed, a subpopulation of cytoplasmic D1 was co-localized with the P-body marker DDX6 (Fig. 7A). Similarly, when overexpressed, N3 protein was found in both the nucleus and cytoplasm; however, N3 did not co-localize with P-bodies in hESCs when D1 was not present (Fig. 7B). Notably, when D1 and N3 were overexpressed simultaneously in hESCs, both D1 and N3 were co-localized in P-bodies (Fig. 7C; Supplementary Fig. 7A, B), suggesting that D1 recruits N3 into P-bodies. This aligns with the observation that D1 promotes N3 binding to their target mRNAs (Fig. 5). Importantly, we also captured the P-body localization of D1 and N3 in hPGCLCs (Supplementary Fig. 7C, D). Given that *SOX4* mRNA is a key downstream target of the D1-N3 complex in hPGCLC induction, we next examined the localization of *SOX4* 3'UTR reporter mRNAs in D1-N3-dOE hESCs using the MS2-based signal amplification with the Suntag system[53] (Supplementary Fig. 7E). Importantly, *SOX4* reporter mRNAs were localized in P-bodies (Fig. 7D; Supplementary Fig. 7F). Together, these results indicate that D1 recruits N3 to P-bodies for regulating the translational level of *SOX4* for hPGCLC development.

To understand how *SOX4* mRNAs are regulated by the D1-N3 complex in P-bodies, we used Cycloheximide (CHX) to disrupt P-bodies in hESCs and examined the effect on SOX4 protein levels (Fig. 7E)[54,55]. CHX treatment alone did not significantly affect SOX4 protein level (Supplementary Fig. 7G). Interestingly, when P-bodies were depleted by CHX treatment, the overexpression of D1-N3 failed to suppress SOX4 protein levels (Fig. 7F), suggesting that the D1-N3 complex functions in P-bodies to regulate the translation of *SOX4*. Importantly, overexpression of D1-N3 decreased SOX4 protein levels (Fig. 6F), however, the protein level of SOX4 was de-repressed when P-bodies were disassembled (Fig. 7G), verifying that P-bodies are critical for D1-N3-mediated repression of *SOX4* translation.

Next, we focused on how the D1-N3 complex represses *SOX4* translation in P-bodies. Given that SOX4 protein levels decreased in hESCs with D1 and N3 overexpressed, but the mRNA levels remained unchanged, we reasoned that D1-N3 triggers translational repression rather than mRNA decay in P-bodies. It has been reported that EIF4E-NIF1 (4E-T) functions with CNOT1 to mediate translational repression, but not mRNA decay, in P-bodies[54]. We next tested whether the D1-N3 complex physically interacts with the 4E-T-CNOT1 complex. Interestingly, D1 interacted with the 4E-T-CNOT1 complex in an RNA-independent manner, and the interaction between D1 and 4E-T was promoted by N3 (Fig. 7H). These observations reveal that N3 is required for D1 to interact with 4E-T to trigger translational repression. If our hypothesis is correct, we would expect that tethering N3 to the 3'UTR of *SOX4* inhibits the translation in the absence of D1 (Fig. 7I). To test this, we cloned 20x BoxB sequence with *SOX4*-3'UTR downstream of Renilla luciferase (Rluc) and define the translation efficiency by normalizing luciferase activity to mRNA level. When N3 was over-expressed in the absence of D1, the translation efficiency of *SOX4*-3'UTR-fused Rluc did not change significantly (Fig. 7J). Importantly, tethering N3 to the 3'UTR of *SOX4* strongly suppressed the translation of Rluc regulated by *SOX4*-3'UTR to about 25% (Fig. 7J). In summary, our results demonstrate that the D1-N3 complex represses the translation of target mRNAs, such as *SOX4*, in P-bodies to restrict the entry of germ cell fate, with D1 being required for the D1-N3 complex to bind to target mRNAs, while N3 is required for the D1-N3 complex to interact with the 4E-T repressor.

Discussion

In this study, we uncovered the collaborative action of PGC-specific RBPs D1 and N3, forming a complex that operates within P-bodies to modulate the translation of *SOX4* mRNA, thereby regulating the induction of germ cell fate from hESCs. Throughout the process of hPGCLC specification from hESCs, D1 binds to target mRNAs and recruits N3 to P-bodies. Within this cellular compartment, the D1-N3 complex interacts with the 4E-T-CNOT1 complex, orchestrating translational repression mechanisms (Fig. 7K). Among the pivotal downstream target mRNAs, *SOX4* emerges as a significant mediator. Previously, we identified SOX4 as a potential key component of the transcription factor network governing hESC to hPGCLC specification[55]. Knockdown of SOX4 leads to decreased percentage of hPGCLCs induced from hESCs (Fig. 6). The D1-N3 complex specifically binds to the 3'UTR of *SOX4* mRNAs, instigating an EIF4E-independent pathway via 4E-T-CNOT1 to repress translation, thereby constraining the initiation of germ cell fate. In scenarios where D1 is absent, N3 fails to bind to target mRNAs within P-bodies, resulting in enhanced translation of *SOX4* mRNA and subsequently increased induction of hPGCLCs. Conversely, in the absence of N3, although D1 binds to target mRNAs within P-bodies, the failure to interact with 4E-T hampers translational repression, consequently leading to increased hPGCLC induction (Fig. 7K).

Notably, using *SOX4* mRNA as a paradigmatic example, we observed unchanged mRNA levels in D1 or N3 mutants, while the protein levels of SOX4 were affected, underscoring the pivotal role of germline-specific RBPs in post-transcriptional regulation, which might account for why the molecular functions of D1 and N3 were not elucidated via RNA-seq or other techniques focused solely on changes at the transcriptional level[27,28,30,56]. More intriguingly, the overexpression of either D1 or N3 alone failed to regulate the translation of *SOX4* mRNAs (Fig. 6), highlighting the importance of the D1-N3 interaction in hPGCLC specification. In mice, the complexes formed between DND1 and NANOS family members are essential for the progressive differentiation of male embryonic germ cells[25,26,57]. These discoveries further emphasize the necessity of investigating the functions of RBPs in complexes during germ cell development. 4E-T-CNOT1 complex

https://doi.org/10.1038/s41467-025-57490-6

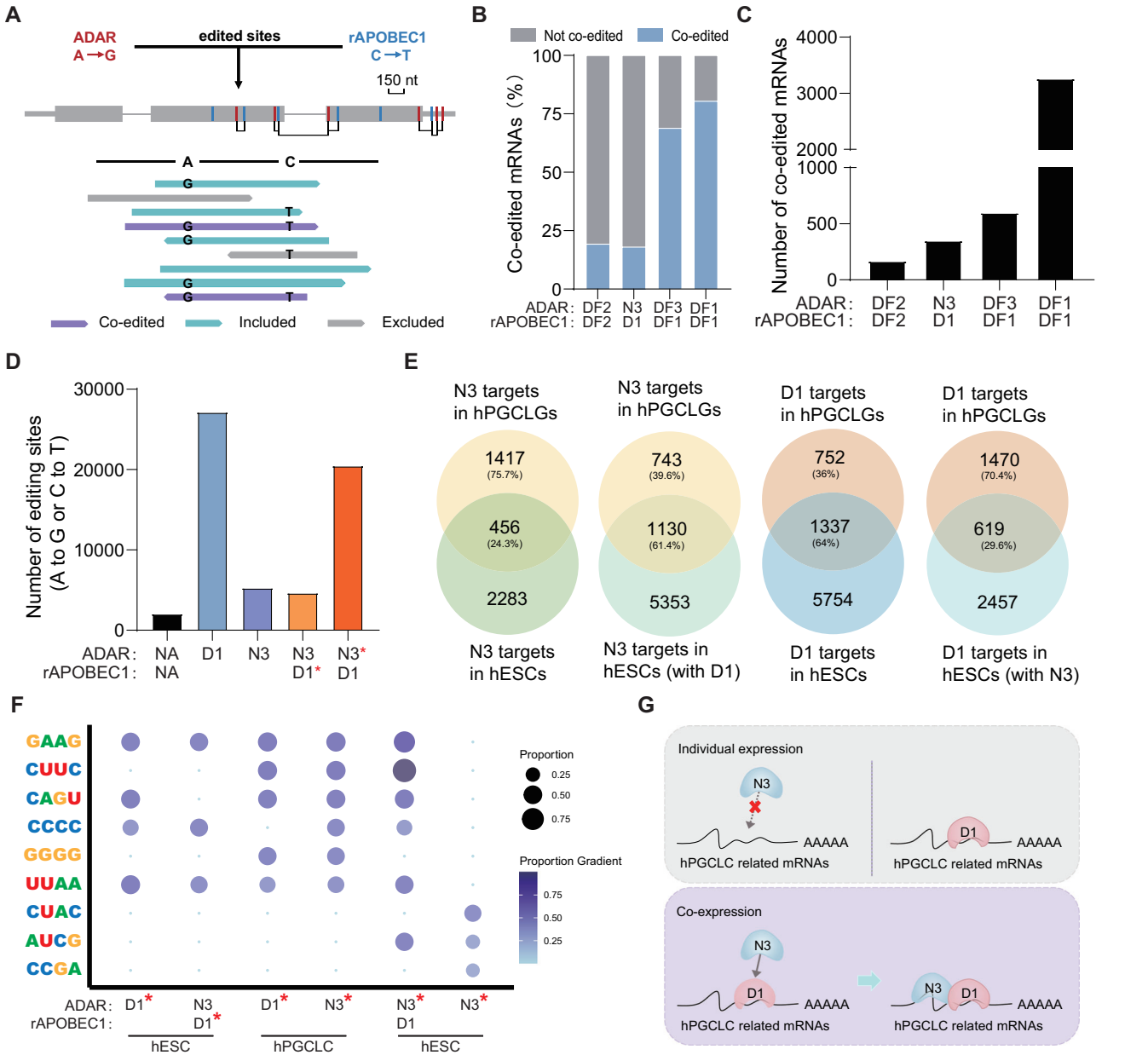

Fig. 5 | D1 recruits N3 to bind to hPGCLC-related target mRNAs. A Schematic illustration showing the workflow for single-molecule TRIBE-STAMP analysis. **B** Proportion of shared target mRNAs with single-molecule co-editing (A–I and C–U) in cells expressing the indicated xx-ADAR and xx-rAPO fusion proteins. Only the shared targets with A–I and C–U editing sites within a 150-nt window on individual reads were considered. **C** Number of mRNAs with single-molecule co-editing (A–I and C–U) in cells expressing the indicated xx-ADAR and xx-rAPO fusion proteins. **D** Bar graph showing the number of editing sites (A–I and C–U) detected in control, *D1-ADAR, N3-ADAR, D1-rAPO + N3-ADAR* hESCs. **E** Venn diagrams showing the overlap of N3 (left two diagrams) and D1 (right two diagrms) target mRNAs in hPGCLCs with target mRNAs identified from hESCs expressing N3 only, D1 only, or N3 + D1. **F** Bubble chart showing the enrichment of corresponding motifs in the target mRNAs of D1 in hESCs, the target mRNAs of N3 in hESCs, the target mRNAs of D1 in *D1-rAPO + N3-ADAR* hESCs, the target mRNAs of N3 in *D1-rAPO + N3-ADAR* hESCs, the target mRNAs of D1 in hPGCLCs, and the target mRNAs of N3 in hPGCLCs. **G** A simplified model showing that D1 drives N3 through interactions to establish binding specificity of hPGCLC-related mRNAs. See also Supplementary Fig. 5.

suppresses the translation of target mRNAs via eIF4A/B/G in an eIF4E-independent mechanism, as previously demonstrated[54]. Intriguingly, inhibition of eIF4A by Zotatifin resulted in decreased SOX4 protein levels in triple-negative breast cancer cells[58], consistent with our findings and indicating tight translational regulation of *SOX4* by the 4E-T-CNOT1-eIF4A/B/G complex.

Germ cells represent the linchpin in perpetuating species, transmitting genetic and epigenetic information from parents to offspring. Specification of PGCs during early embryogenesis constitutes the foremost and most crucial step in establishing the germ cell lineage. The advent of in vitro hPGCLC induction systems has propelled extensive research into the mechanisms underlying hPGCLC specification from hESCs, leading to the identification of key germ cell fate determinants such as TFAP2C, SOX17, PRDM1, and EOMES. Notably, all these factors serve as positive regulators of germ cell fate specification. Although germ cells are vital for species continuity, excessive germ cell induction during early embryogenesis, at the expense of somatic cells, can culminate in abnormal development. Consequently, precisely controlled mechanisms are essential to restrain the induction of germ cell fate and maintain the balance between germ cells and somatic cells. The D1-N3 complex serves as a crucial "braking system" tasked with restricting germ cell specification to maintain this delicate

https://doi.org/10.1038/s41467-025-57490-6

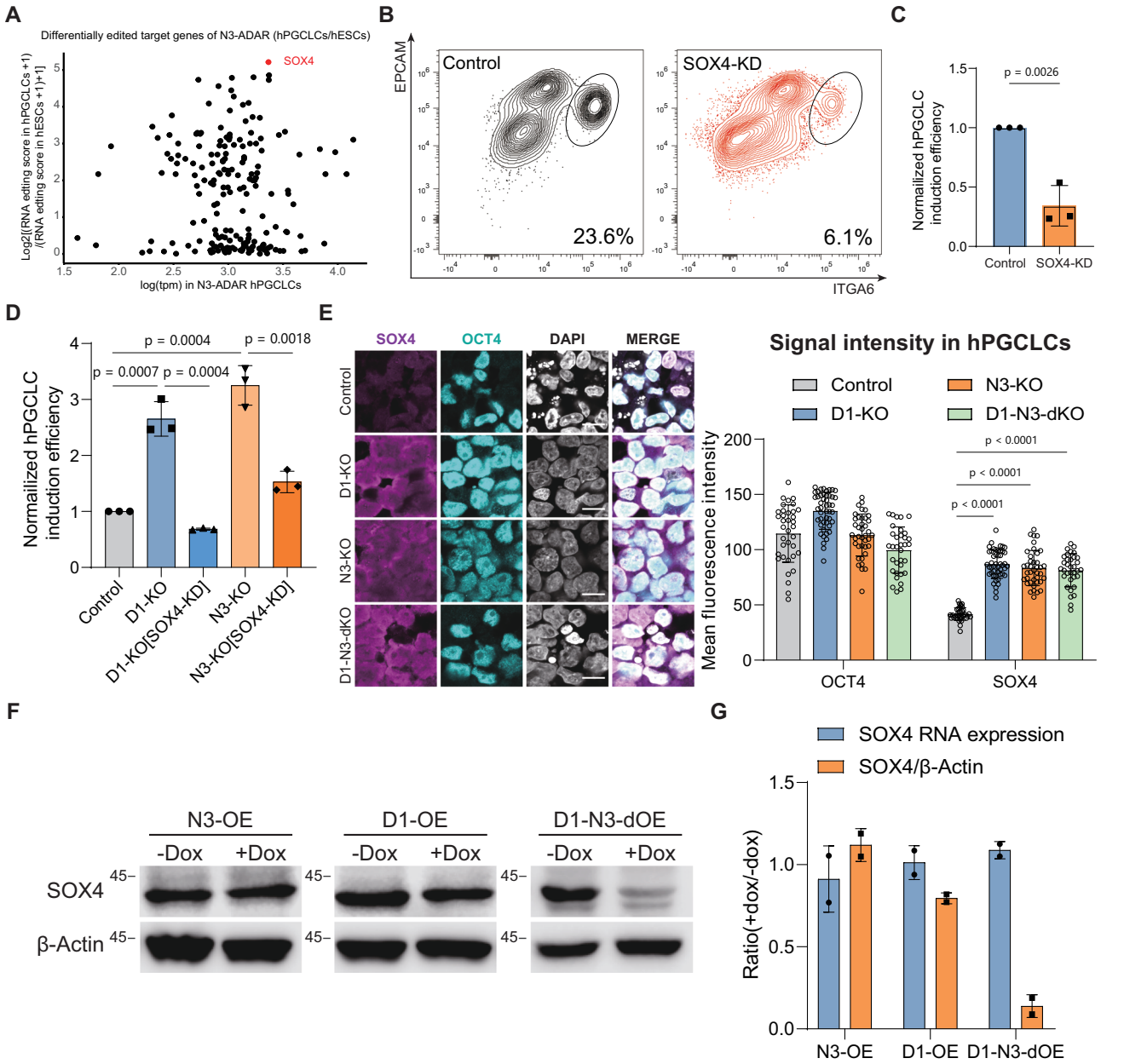

Fig. 6 | D1 and N3 restrict the induction of hPGCLCs by regulating the translation of SOX4. A Scatter plot showing the differentially edited target genes of N3-ADAR (the 187 mRNA targets in Supplementary Fig. 6A) by comparing the RNA editing scores in hPGCLCs to N3-only hESCs (y axis), and the expression levels of these target mRNAs in hPGCLCs (x axis). **B** FACS analysis showing the percentages of day 4 hPGCLCs induced from control and *SOX4* knock-down hESCs. Greg: control; Red: *SOX4* knock-down. **C** Statistics of normalized hPGCLC percentages from control and *SOX4* knock-down hESCs. Mean with SD from n = 3 experiments. Unpaired t test; two-tailed P value. Source data are provided as a Source Data file. **D** Statistics of normalized hPGCLC percentages from control, *D1-KO*, *D1-KO* + *SOX4* knock-down, *N3-KO,* and *N3-KO* + *SOX4* knock-down hESCs. Mean with SD from n = 3 experiments. Unpaired t test; two-tailed P value. Source data are provided as a Source Data file. **E** Left: Immunofluorescence showing the signal intensity of SOX4 protein (magenta), OCT4 (cyan), and DAPI (gray) in control, *D1-KO*, *N3-KO*, and *D1-N3-dKO* day 4 hPGCLC aggregates. Scale bar: 5 μm. Right: Evaluation of the mean signal intensity of OCT4 proteins and SOX4 proteins within hPGCLCs in control, *D1-KO*, *N3-KO,* and *D1-N3-dKO* groups. Data are presented as Mean with SD. Significance was determined using Mann-Whitney U test; two-tailed P value. Control: n = 36 cells, *D1-KO*: n = 47 cells, *N3-KO*: n = 39 cells, *D1-N3-dKO*: n = 34 cells. Quantification was based on confocal images of at least 3 independent aggregates for each group. Source data are provided as a Source Data file. **F** West Blot showing the protein levels of SOX4 in N3-OE, D1-OE, and D1-N3-dOE hESCs and their corresponding control hESCs. β-Actin serves as loading control. Source data are provided as a Source Data file. **G** Bar graph showing the relative levels of *SOX4* mRNAs and SOX4 proteins in N3-OE, D1-OE, and D1-N3-dOE hESCs. Mean with SD from n = 2 experiments. Source data are provided as a Source Data file. See also Supplementary Fig. 6.

balance. Given that not all hESCs develop into hPGCLCs, it is possible that additional "braking systems" exist to repress germ cell fate. Thus far, the transcription factor OTX2 is the sole factor characterized as a repressor of human germ cell fate[59,60]. In Drosophila, the RBP Smaug functions similarly as a repressor to restrict the specification of PGCs by inhibiting the translation of target mRNAs in germ granules[61,62]. The identification of more repressors for germline entry will provide insights into how the balance between germ cells and somatic cells is orchestrated and how disruptions in this balance may contribute to fertility-related diseases and birth defects.

Although the molecular functions of D1 and N3 have been extensively studied in model organisms[17,20,23,24,32,35,36,41], their key target

https://doi.org/10.1038/s41467-025-57490-6

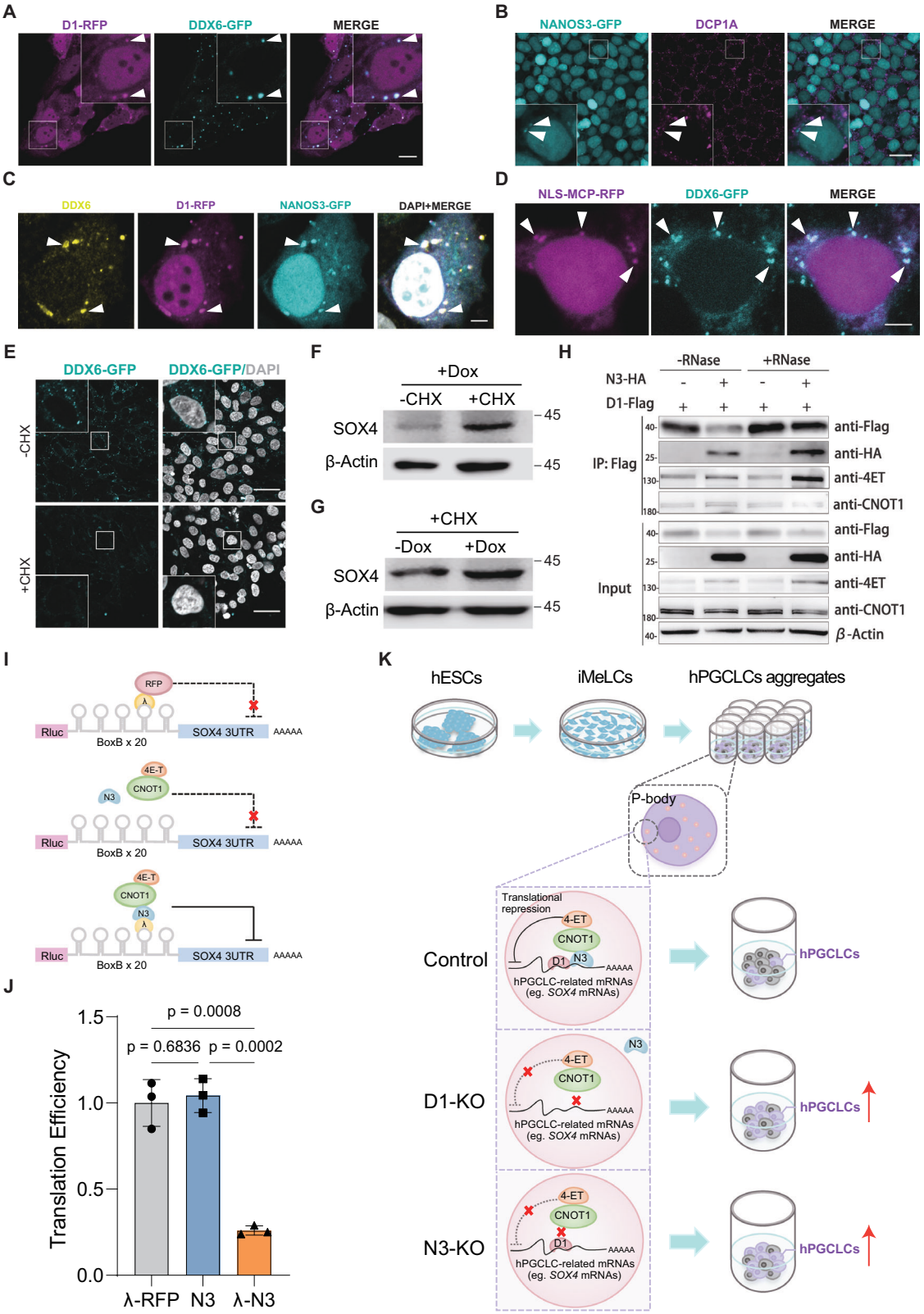

mRNAs in PGCs remain largely elusive. In this study, we identified *SOX4* mRNA as a critical regulated target of the D1-N3 complex, modulating germline entry. Despite the decreased protein levels of SOX4 upon expression of D1 and N3, the mRNA levels of *SOX4* remained unaltered. This may explain why previous studies failed to identify key functional downstream effectors based solely on RNA level changes. D1 and N3 may exhibit different roles in humans compared to mice, as proteins often function differentially across organisms[63]. Notably, even for the D1 protein itself, Dnd1Ter mutants exhibit germ cell tumors and deletion of D1 leads to PGC apoptosis in mice[35,64,65], while depletion of D1 in zebrafish results in the trans-differentiation of PGCs to somatic cells[24], underscoring species-specific functions of D1 in regulating PGCs. In humans, we identified the D1-N3 complex as a critical regulatory barrier to suppress the

Fig. 7 | P-bodies are essential for D1-N3 complex to repress the translation of *SOX4*. **A** Fluorescence observation of D1-RFP (magenta) and DDX6-GFP (cyan) in hESCs. Scale bar: 5 μm. Representative images from three independent experiments. **B** Immunofluorescence of N3-GFP (cyan) and DCP1A (magenta) in hESCs. Scale bar: 10 μm. Representative images from three independent experiments. **C** Immunofluorescence of DDX6 (yellow) and D1-RFP (magenta) and N3-GFP (Cyan) in hESCs. Scale bar: 2 μm. Representative images from three independent experiments. **D** Fluorescence observation of nls-MCP-RFP (magenta) and DDX6-GFP (cyan) in D1-N3-dOE hESCs with Dox. Scale bar: 2 μm. Representative images from three independent experiments. **E** Examination of DDX6-GFP (cyan) in hESCs without and with CHX treatment for 20 h. DAPI (gray) is counterstained to indicate nuclei. Scale bar: 20 μm. Representative images from three independent experiments. **F** Western blot showing the protein level of SOX4 for Dox-inducible expression of D1-N3 in the presence of CHX. Dox and CHX were added simultaneously. +Dox indicates over-expression of both D1 and N3. β-Actin serves as loading control. Representative images from three independent experiments. Source data are provided as a Source Data file. **G** Western blot showing the protein level of SOX4 in D1-N3 over-expressed hESCs in the absence or presence of CHX. Dox and CHX were added simultaneously. β-Actin serves as loading control. Representative images from three independent experiments. Source data are provided as a Source Data file. **H** Co-immunoprecipitation assay showing the physical interaction of D1 with N3, 4E-T, and CNOT1 with and without RNase treatment. Representative images from three independent experiments. Source data are provided as a Source Data file. **I** Schematic illustration of the Rluc-BoxB tethering reporter system. **J** Tethering assay showing the normalized Rluc activity in λN-RFP, N3, and λN-N3 groups. Renilla luciferase (Rluc) activity is normalized to firefly luciferase (Fluc) activity. Rluc-SOX4 3′UTR mRNA level is quantified by RT-qPCR and normalized to Fluc mRNA. The translation efficiency is calculated as the ratio of normalized Rluc activity to the normalized Rluc-SOX4 3′UTR mRNA level. Mean with SD from n = 3 experiments. Unpaired t test; two-tailed P value. Source data are provided as a Source Data file. **K** A proposed model showing that D1 and N3 coordinately suppress the translation of *SOX4* via 4E-T in processing bodies for restricting the entry of germ cell lineage. See also Supplementary Fig. 7.

entry of the germ cell lineage, actively balancing cell fate allocation during early embryogenesis.

P-bodies, classic membraneless organelles in eukaryotic cells, serve as the site for 4E-T-CNOT1 complex recruitment in D1-N3-mediated translational repression. Although P-bodies may exist in all cell types for RNA decay, storage, surveillance, and translational repression[66–68], their involvement in developmental regulation remains largely enigmatic. Prior research has highlighted the importance of P-bodies in maintaining the pluripotent state and differentiation capacities of human induced pluripotent stem cells (iPSCs)[69]. However, whether P-bodies exhibit heterogeneity in composition and whether this correlates with cell-type-specific regulation remains unexplored. In this study, we discovered that D1-N3 complex localizes in P-bodies. Given that D1 and N3 are only expressed in germ cells, our observations highlight the cell-type-specific composition of P-bodies. More importantly, germ cell-specific D1 and N3 are critical factors for regulating germ cell fate, highlighting the potential critical roles for P-bodies in developmental regulation. Identification of more cell-type-specific components of P-bodies will help us understand more about how P-bodies are involved in the regulation of different biological processes.

Methods

Cell culture and drug treatments

HEK293 cells were cultured in high-glucose Dulbecco's modified eagle medium (DMEM) (TransGen Biotech, FI101-01) supplemented with 10% (v/v) fetal bovine serum (FBS) (ExcelBio, FSP500) and 50 ng/ml Primocin (InvivoGen, ant-pm-2). H1 (WiCell, Cat#WA01-pcbc), H9 (WiCell, Cat#WA09-pcbc), HN4 (from Duanqing Pei Lab at Westlake University) hESCs were cultured in the Nuwacell® ncTarget hPSC medium (Nuwacell, RP01020) supplemented with 50 ng/mL Primocin (InvivoGen, ant-pm-2). Cells were cultured at 37 °C with 5% CO_2. Mycoplasma test was performed biweekly. For the inducible expression of target genes, cells were cultured with 1 mg/mL of Dox (Selleck, S5159) in the culture medium. For drug selection, 1 μg/mL Puromycin (Selleck, S7417), 4 μg/mL Blasticidin (Solarbio, B9300), 2 μM/mL Ganciclovir (MCE, 82410-32-0) and 10 μM Y-27632 (Selleck, S1049) were added to the culture medium.

hESC culture

H1 (46, XY), H9 (46, XX) and HN4 (46, XX) hESCs were cultured in Nuwacell® ncTarget hPSC medium (Nuwacell, RP01020) supplemented with 50 ng/mL Primocin (InvivoGen, ant-pm-2) on Matrigel (Corning, 354234)-coated plates. The cells were maintained at 37 °C with 5% CO_2. The medium was changed every other day. Cells were passaged with Dispase (STEMCELL, 07923) when they were ~80% confluence.

For the induction of iMeLCs and hPGCLCs, hESCs were cultured on irradiated mouse embryonic fibroblasts (MEFs) in basic DMEM/F-12 (1:1) medium (GIBCO, C11330500BT) supplemented with 20% KnockOut Serum (GIBCO, 10828028), 1% non-essential amino acids (GIBCO, 11140-050), 0.1 nM β-mercaptoethanol (GIBCO, 21985023), 1× Penicillin-Streptomycin-Glutamine (Invitrogen, 10378016) and 10 ng/mL FGF2 (Peprotech, 100-18B). Cells were maintained at 37 °C with 5% CO_2. The medium was changed every other day. The cells were passaged with Dispase (STEMCELL, 07923) when they were ~80% confluence.

hPGCLC induction

For the induction of iMeLCs, hESCs were dissociated with ACCUTASE (STEMCELL, 07992) and filtered with a 40 μm cell filter (JET, CSS013040), and 4.0×10^5 cells/12-well were plated on human plasma fibronectin (Invitrogen, 33016015)-coated plates in the GK15 medium [GMEM (GIBCO, 11710-035) with 15% KSR (GIBCO, 10828028), 0.1 mM NEAA, 1× Penicillin-Streptomycin-Glutamine (Invitrogen, 10378016), 1 mM sodium pyruvate (GIBCO, 11360070), and 0.1 mM 2-mercaptoethanol (GIBCO, 21985023)] supplemented with 50 ng/mL Activin A (ACTA) (Peprotech, AF120-14E), 3 μM CHIR99021 (Stemgent, 04000410) and 10 μM Y-27632 (Selleck, S1049). After 24 h, the iMeLCs were dissociated with ACCUTASE (STEMCELL, 07992) and were aggregated in an Anti-Adherence Rinsing Solution (STEMCELL, 07010)-coated U-bottom 96-well plate (JET, TCP012096) at 4.0×10^5 cells per well in the GK15 medium supplemented with 200 ng/ml BMP4 (R&D Systems, 314-BP-01M), 50 ng/mL EGF (R&D Systems, 236-EG-01M), 10 μg/mL of Human LIF (Millipore, LIF1005), and 10 μM of Y-27632 (Selleck, S1049) to induce hPGCLCs.

Fluorescence activated cell sorting (FACS)

For hESC detection, cells were dissociated with ACCUTASE (STEMCELL, 07992), blocked with 5% BSA for 15 min at 4 °C, and incubated with AF488-conjugated SSEA4 antibody (Cell Signaling Technology, 4755T) for 15 min at 4 °C. The cells were centrifuged at 200 × *g* for 5 min at 4 °C and were resuspended in FACS buffer containing 7AAD (Beyotime, ST515, 1:200), then were analyzed by NovoCyte™ flow cytometry (ACEA).

For hPGCLC detection, the aggregates were collected at the designated days and dissociated with 0.05% Trypsin (GIBCO, 25300054) for 10 min at 37 °C and dispersed by gentle pipetting. After washing with DMEM (TransGen Biotech, FI101-01) containing FBS, the cells were suspended in FACS buffer (0.1% BSA in PBS), then stained with BV421-conjugated anti-CD49f (INTEGRINα6) antibody (BioLegend, 313624, 1:100) and APC-conjugated anti-CD326 (EpCAM) antibody (BioLegend, 324207, 1:100) or AF488-conjugated anti-CD326 (EpCAM) antibody (BioLegend, 324210, 1:100) in FACS buffer. After

incubation on ice for 15 min, 1 mL of FACS buffer was added to the sample and then centrifuged at 200 × *g* for 5 min at 4 °C. Discard the supernatant and resuspend the cell pellet in FACS buffer containing 7AAD (Beyotime, ST515, 1:200). The cells were processed by BD Influx™ Cell Sorter (BD Biosciences) for analysis and sorting.

Knock-out hESC line generation

For *DND1* and *NANOS3* genes knock-out, guide RNAs (gRNAs) were designed by CHOPCHOP and cloned into the PX459 vector (Addgene, 62988). For *NANOS3*, a donor vector with homology arms and the puromycin resistance sequence for drug selection was generated as depicted in Supplementary Fig. 2C. The thymidine kinase (TK) sequence was inserted to exclude random insertion. 4 μg of gRNA pairs and 4 μg donor vectors were electroporated into 8.0×10^5 hESCs using the P3 Primary Cell 4D-Nucleofector X Kit (Lonza, V4XP-3024) on 4D-nucleofector (program CA137, Lonza) following the manufacturer's instructions. 24 h or more after nucleofection, cells were dissociated with ACCUTASE (STEMCELL, 07992) and seeded on a Matrigel (Corning, 354234)-coated 6-well plate for drug selection with 1 μg/mL Puromycin (Selleck, S7417), 2 μM/ml Ganciclovir (MCE, 82410-32-0) and 10 μM Y-27632 (Selleck, S1049) in Nuwacell® ncTarget hPSC Medium (Nuwacell, RP01020). After selection, cells were passaged at low density into Matrigel-coated 10 cm^2 dish. After 10 days, 96 colonies were picked and expanded for screening. Genomic DNA was extracted from 96 colonies using the FastPure Cell/Tissue DNA Isolation Mini Kit (Vazyme, DC102-01) and identified by genotyping PCR. For selected colonies, mutant bands were amplified and sequenced to determine the precise mutant locus. The gRNAs and genotyping primers are listed in Supplementary Table 1.

Inducible expressing hESC line generation

For lentivirus production, ~90% confluent HEK293T cells were transfected with tet-ON system-based expression vectors, along with the lentiviral packaging plasmids pMD2.G (Addgene, 12259) and psPAX2 (Addgene, 12260) in a 3.2 μg:0.8 μg:2.4 μg ratio, using 5 μL of 1 mg/mL PEI solution (polysciences, 24765100). 72 hr after transfection, the lentiviral supernatant was collected with 10% PEG 8000 (Solarbio, P8260) and filtered by 0.45 μm syringe filters (Millipore, SLHU033RB). After concentrating at 4 °C overnight, the mixture was centrifuged at 4000 × *g* at 4 °C for 25 min. The precipitate was resuspended by PBS and used as the lentivirus solution. For hESC infection, the lentivirus solution was transduced into hESCs dissociated into single cells with 10 μg/ml polybrene (Sigma, H9268) and 10 μM Y-27632 (Selleck, S1049). After rotating for 2 hr, cells were seeded into Matrigel (Corning, 354234)-coated plates. Monoclonal cell lines were screened as described above, and the selected clones were identified by PCR, western blot, RT-qPCR, or immunofluorescent staining. For generating the D1/N3 rescue hESCs (Fig. 1 and Fig. 2) and D1/N3 overexpressing hESCs (Fig. 3), the titers of the lentiviruses were adjusted to ensure that approximately half of the hESCs were positive (expressing the target gene), while the other half remained negative (control cells).

Knock-down hESC line generation

The gRNA vector was co-transfected with pMD2.G (Addgene, 12259) and psPAX2 (Addgene, 12260) into HEK293T cells to generate the lentiviruses. For CRISPRi cell line generation, pZT-C13-L1 (Addgene, 62196), pZT-C13-R1 (Addgene, 62197), and pC13N-dCas9-BFP-KRAB (Addgene, 127968) were electroporated into 8.0×10^5 hESCs using the P3 Primary Cell 4D-Nucleofector X Kit (Lonza, V4XP-3024) on 4D-nucleofector (program CA137, Lonza) following manufacturer's instructions. 4 μg of each plasmid was used for nucleofection. After expansion, BFP-positive hESCs were collected by sorting at about 70–80% confluency using a gentle dissociation method. After three rounds of sorting, BFP-positive hESCs reached 100% positive rate. Lentiviruses containing SOX4-targeted dual-gRNA were transduced into this CRISPRi hESC line. The titers of the lentiviruses were adjusted to ensure that approximately half of the hESCs were positive (expressing the gRNA), while the other half remained negative (control cells).

Plasmid construction

Expression vectors. The full-length coding sequences (CDSs) of the target genes *DND1, NANOS3, DDX6, 4E-T*, and the following sequence including *FLAG, HA, GFP, RFP*, and *ADAR* were amplified utilizing Phanta Max Super-Fidelity DNA Polymerase (Vazyme, PD505). The fragments and EcoRI-linearized pFUW-tetO-loxP-hNANOG vectors (Addgene, #60849) were fused using the ClonExpress II One Step Cloning Kit (Vazyme, C11202) to generate pFUW-tetO-HA/FLAG-hDND1, pFUW-tetO-NANOS3-HA/FLAG, pFUW-tetO-DND1-ADAR-V5, pFUW-tetO-NANOS3-ADAR-V5, pFUW-tetO-NANOS3-GFP/RFP, pFUW-tetO-hDND1-GFP/RFP, pFUW-tetO-DDX6-GFP, and pFUW-tetO-4E-T-HA plasmids. The sequences for ADAR were described previously[42].

MS2-MCP vectors. To generate the pFUW-tetO-BFP-SOX4 3'UTR-MS2 plasmid, the 3' untranslated region (UTR) of *SOX4* was amplified from human cDNAs and cloned into EcoRI-linearized pFUW-tetO-loxP-hNANOG with BFP and MS2. To generate the pFUW-tetO-nls-tdMCP-24xGCN4 plasmid, the NLS sequence was cloned into EcoRI-linearized pFUW-tetO-loxP-hNANOG followed by replacing the hNANOG sequence with the tdMCP-24xGCN4 sequence. To generate the pFUW-tetO-scfv-GCN4-mCherry-GB1 plasmid, scfv-GCN4, Cherry, and GB1 were amplified and cloned into EcoRI-linearized pFUW-tetO-loxP-hNANOG. The sequences of MS2, tdMCP-24xGCN4, scfv-GCN4 and GB1 were described previously[53,70].

Luciferase vectors. To generate the pCMV-myc-λN-NANOS3 plasmid, *NANOS3* CDS was amplified and inserted into the pCMV-Myc-λN-mCherry vector[71] using XhoI restriction sites. To generate the pRL-SV40-MS2-20xBoxB-SOX4 3'UTR plasmid, the *SOX4* 3'UTR was amplified and inserted into the NotI site of the pRL-SV40-MS2-20xBoxB vector[71].

Knockdown gRNA vectors. For the construction of the CRISPRi knockdown plasmids targeting *SOX4*, two gRNAs were designed based on the CRISPRi gRNA pool list from Jonathan Lab[72]. The two gRNA sequences were incorporated into the amplification primers and fused respectively to the C-terminus of the U6 promoter and H1 promoter. The ClonExpress II One Step Cloning Kit (Vazyme, C11202) was utilized to ligate the gRNA1-U6 promoter-H1 promoter-gRNA2 fragment with the BbSI-linearized-pLenti-U6-EF1a-mCherry vector to generate the pLenti-U6-H1-gRNAs-EF1a-mCherry vector plasmid. The pLenti-U6-EF1a-mCherry vector was generously provided by the Chan Lab. The gRNA sequences were:

5′-GGGCCGCGAGAAACTTGCAT-3′, 5′- GAGACCGTGCTAAAGTAGAG-3′.

All recombinant DNA, their sources are listed in Supplementary Table 2.

Co-immunoprecipitation

For co-immunoprecipitation, the collected cells were washed once with PBS (Solarbio, 49900532) and lysed with RIPA Lysis Buffer (Beyotime, P0013C), followed by the addition of protease inhibitors Aprotinin (1 μg/mL), Leupeptin (1 μg/mL), Pepstatin (1 μg/mL), and PMSF (1 mM). The mixture was lysed for 30 min at 4 °C on a rotation wheel. The supernatant was obtained as Whole Cell Lysate (WCL) through centrifugation at 13,523 × *g* for 7 min at 4 °C. A portion of WCL was mixed with 4X SDS Loading Buffer (BBI life sciences, A600485-0500) as Input sample. The remaining WCL was incubated with pre-prepared agarose beads (HA: Smart-Lifesciences, SA068001; FLAG: Selleck, B26101) for 4 h at 4 °C under rotation. Afterward, the beads

were washed three times and then mixed with 2X SDS Loading Buffer (BBI life sciences, A600485-0500) as IP sample. Both Input and IP samples were denatured by heating at 100 °C for 10–20 min and then used for protein immunoblotting. For the RNase A-treated samples, the procedure remained the same, except that RNase A was included in the lysis buffer.

Western blotting

For Western Blot, after the collected cells were washed with PBS (CHEM17, M10201) and lysed in 4X SDS Loading Buffer (BBI life sciences, A600485-0500). The mixture was then heated at 100 °C for 10–20 min. Proteins were separated using an 8–12% SDS-PAGE gel under constant voltage of 160 V with 1X Electrophoresis Buffer, and then transferred to PVDF membranes (Millipore, IPVH00010) at a constant current of 300 mA for 100 min in 1X Transfer Buffer. Membranes were blocked with 5% skim milk for 1 h at room temperature, washed with TBST, and incubated overnight at 4 °C with primary antibodies diluted in 3% BSA (Sangon, A500023-0100) at a 1:2000 ratio. The primary antibodies used included: Mouse anti-human β-actin (HuaBio, EM21002), SOX4 Polyclonal Antibody (Bioswamp, PAB37141), Rabbit anti-human HA (HuaBio, 0906-1), Mouse anti-human FLAG (HuaBio, M1304-2), Rabbit anti-human GFP (HuaBio, ET1607-31), Mouse anti-human V5 (Sigma, V8012), and CNOT1 Polyclonal Antibody (Bioswamp, PAB41896). The next day, membranes were incubated with HRP-conjugated secondary antibodies diluted in 5% skim milk at a 1:2000 ratio (HRP-linked anti-rabbit IgG, CST, 7074P2; HRP-linked anti-mouse IgG, CST, 7076P2) for 2 h at room temperature. Membranes were washed with TBST and visualized using enhanced chemiluminescence reagent (ECL) (Advansta, K-12045-D50). ImageJ software was used for analysis.

Immunofluorescence

For cells in dishes, cells were cultured in 35-mm glass-bottom dishes (NEST, 704001), washed with PBS (Solarbio, 49900532), fixed with 4% PFA (Biosharp, BL539A) for 15 min in the dark. Cells were permeabilized with 0.1% Triton X-100 (Sigma, V900502) for 15 min at room temperature, and then blocked by incubating with 5% BSA (Sangon, A500023-0100) for 1 h at room temperature. Subsequently, cells were incubated overnight with primary antibodies at 4 °C in a humidified chamber. The next day, cells were incubated with secondary antibodies for 2 h at room temperature, followed by DAPI (Beyotime, C1002) staining for 10 min at room temperature. Cells were washed three times with PBS and mounted with Antifade Mounting Medium (Beyotime, P0126). Images were captured using an LSM 880 Confocal Microscope (Zeiss) and analyzed with ZEN software.

For OCT sections, aggregates were embedded in Optimal Cutting Temperature Compound (OCT) (SAKURA, 4583) and sectioned at 8 μm thickness. Sections were washed three times with PBS (Solarbio, 49900532) for 5 min each, circled with a PAP Pen (Biosharp, BC004), and fixed in 4% PFA (Biosharp, BL539A) for 15 min in the dark. Sections were permeabilized with 0.1% Triton X-100 (Sigma, V900502) for 15 min at room temperature and blocked with 5% BSA (Sangon, A500023-0100) for 1 h at room temperature. Primary antibodies were added, and sections were incubated overnight at 4 °C in a humidified chamber. The next day, sections were incubated with secondary antibodies for 2 h at room temperature, followed by DAPI staining for 10 min. Sections were washed three times with PBS, mounted with Antifade Mounting Medium (Beyotime, P0126), and sealed with a cover glass. Images were captured using an LSM 880 Confocal Microscope (Zeiss) and analyzed with ZEN software. All antibodies, their sources are listed in Supplementary Table 3.

RT-qPCR

Total RNA was isolated from cells using the AG RNAex Pro Reagent (Accurate Biology, AG21101), and mRNA was reverse transcribed into cDNA by Evo M-MLV RT Premix (Accurate Biology, AG11706). The obtained cDNA was mixed with 2X SYBR Green Pro Taq HS Premix (Accurate Biology, AG11701), sterile water and primers to form a reverse transcription system. Transcript expression was assessed by subjecting synthesized cDNA to quantitative PCR using a CFX96 Touch Real-Time PCR Detection System (Bio-Rad). GAPDH gene expression level was used as an internal reference. After the reaction, the amplification and melting curves were confirmed and analyzed. All qPCR primers are listed in Supplementary Table 4.

EdU incorporation assay

Cell proliferation was assessed using a 5-ethynyl-20-deoxyuridine (EdU) assay kit (Sangon Biotech, E6072040100). For control and *NANOS3-KO* hESCs, cells cultured to ~70% confluence were incubated with the EdU Cell Proliferation Kit for 2 h and then nuclear-stained with Hoechst dye. Images were captured with a Zeiss LSM880 microscope and processed by Zen Blue software. The number of total cells and cells with proliferative activity in the field of view were counted in ImageJ software.

For control, *DND1-KO* and *NANOS3-KO* hPGCLCs, the cell aggregates on day 4 were incubated with the EdU Cell Proliferation Kit for 4 h and were collected for cryo-embedding as described previously. Immunostaining co-stained SOX17 and OCT4 to label hPGCLCs, and DAPI stained nuclei. Images were taken with a Zeiss LSM880 microscope. All images were processed by Zen Blue software. The number of total cells and hPGCLCs in the field of view and the number of hPGCLCs with proliferative activity were counted in ImageJ software.

Annexin V assay

The apoptotic activity of control, *DND1-KO* and *NANOS3-KO* cells was evaluated using a FITC Annexin V Apoptosis Detection Kit (BD Biosciences, 556547). Cells were dissociated with ACCUTASE (STEMCELL, 07992), washed twice with cold PBS and resuspended in 1X binding buffer at a concentration of 1.0×10^6 cells/ml. 5 μl FITC Annexin V and 5 μl PI were added to 100 μl of solution (1.0×10^5 cells). Vortex cells gently and incubated for 15 min at room temperature (25 °C) in the dark. Add 400 μl 1X Binding Buffer to each tube. The cells were analyzed by NovoCyte™ flow cytometry (ACEA) within 1 h.

Embryonic body in vitro differentiation

hESCs cultured on Matrigel (Corning, 354234)-coated plates were dissociated with collagenase IV (Gibco, 17104019) for 30 min at 37 °C. The cells were resuspended on low adsorption plates in EB differential medium [DMEM/F12 + 20% Fetal Bovine Serum (FBS, Gibco) + 1% L-GlutaMax (Gibco) + 1% NEAA (Gibco) + 0.1% β-mercaptoethanol (Gibco)] for 10 days.

Luciferase reporter assay

HEK293T cells were seeded on 12-well plates to 90% confluence before usage. The cells were transfected with luciferase reporter plasmid and effector plasmid using PEI solution (polysciences, 24765100) for 24 h. Luciferase activity was detected by Dual Luciferase Reporter Gene Assay Kit (Beyotime, RG028) following the manufacturer's instructions. Renilla luciferase (Rluc) activity is normalized to firefly luciferase (Fluc) activity, and the ratios were calculated to assess the roles of λN-fusion proteins in the regulation of luciferase translation.

Mesoderm, endoderm, and ectoderm induction

For mesoderm induction, on day 0, hESC colonies were harvested and seeded as single cells at a density of $5 \times 10^4/cm^2$ in Nuwacell® ncTarget hPSC Medium (Nuwacell, RP01020) and supplemented with 10 μM Y-27632 (Selleck, S1049). On day 1, when cells reached ~20–50% confluence, the medium was replaced with STEMdiff™ Mesoderm Induction Medium (STEMCELL, 05220). The cells were then fed daily and

cultured in STEMdiff™ Mesoderm Induction Medium (STEMCELL, 05220) (days 2–4). Cells were collected on day 5 for analysis.

For endoderm induction, on day 0, hESC colonies were harvested and seeded as single cells at a density of $5 \times 10^4/cm^2$ in Nuwacell® ncTarget hPSC Medium (Nuwacell, RP01020) and supplemented with 10 μM Y-27632 (Selleck, S1049). On day 1, when cells reached ~20–50% confluence, the medium was replaced with STEMdiff™ Definitive Endoderm Medium (STEMCELL, 05110). The cells were then fed daily and cultured in STEMdiffTM Definitive Endoderm Medium (STEMCELL, 05110) (days 2–4). Cells were collected on day 5 for analysis.

For ectoderm induction, on day 0, hESC colonies were harvested and seeded as single cells at a density of $2 \times 10^5/cm^2$ in STEMdiff™ Neural Induction Medium supplemented with SMADi (STEMCELL, 08581) and 10 μM Y-27632 (Selleck, S1049). The cells were then fed daily and cultured in STEMdiff™ Neural Induction Medium supplemented with SMADi (STEMCELL, 08581) (days 1–5). On day 6, cells were harvested and seeded as single cells at $2 \times 105/cm^2$ in STEMdiff™ Neural Induction Medium supplemented with SMADi (STEMCELL, 08581). The cells were then fed daily and cultured in STEMdiff™ Neural Induction Medium supplemented with SMADi (STEMCELL, 08581) (days 7–12). Cells were collected on day 13 for analysis.

RNA-seq with low cell number

RNeasy Micro Kit (QIAGEN, 74004) was used to extract RNA for PGCLCs. Briefly, on day 4, PGCLCs were sorted directly into 350 μl RLT buffer by FACS for lysis. 350 μl 70% ethanol was then added to each reaction. The mixture was transferred into the RNeasy MinElute spin column for RNA enrichment, followed by two rounds of washing and elution. To enrich mRNA from extracted total RNA, VAHTS mRNA Capture Beads (Vazyme, N401) were applied. After enrichment, VAHTS Universal V8 RNA-seq Library Prep Kit for Illumina (Vazyme, NR605) was utilized to prepare libraries for sequencing, which contains fragmentation, cDNA synthesis, adapter ligation, PCR amplification, and purification. RNA sequencing was performed on NovoSeq 6000 (Illumina) with the PE150 mode.

Bulk RNA-seq

Total RNA was isolated from cells using the AG RNAex Pro Reagent (Accurate Biology, AG21101). After the RNA sample passes the test, magnetic beads with Oligo(dT) are used to enrich eukaryotic mRNA. Then fragmentation buffer is added to break the mRNA into short fragments. Using the mRNA as a template, six-base random primers (random hexamers) are used to synthesize one-strand cDNA. Then buffer, dNTPs, and DNA polymerase I and RNase H are added to synthesize two-strand cDNA. Double-stranded cDNA was then purified using AMPure XP beads. The purified double-stranded cDNA is first subjected to end repair, A-tailing and ligation of sequencing adapters, and then AMPure XP beads are used for fragment size selection. Finally, PCR amplification was performed, and the PCR product was purified with AMPure XP beads to obtain the final sequencing library. RNA sequencing was performed on NovoSeq 6000 (Illumina) with the PE150 mode.

RNA-seq analysis

Quality assessment of the raw RNA-seq data was conducted using FastQC (v0.11.9), which examined the overall quality of the bulk RNA-seq fastq files. After that, cutadapt (v4.1) and trim-galore (v0.6.7) were used to remove low-quality bases and potential adapters. The processed reads were then aligned to the hg38 reference using STAR (v2.7.10a), sorted using samtools (v1.6), and the read counts per gene were quantified through featureCounts (v2.0.1) using the Gencode (v41) genomic annotation file. Subsequently, the differential gene expression analysis was conducted using DESeq2 (v1.40.2) within the R (v4.3.1) environment. The read count matrix was input into DESeq2 for normalization and variance stabilization transformation. The criteria for significant differential gene expression were set as an adjusted p-value less than 0.05 and an absolute log fold change greater than 2. Finally, the results were visualized using ggplot2 (v3.4.4) and ComplexHeatmap (v2.15.4). Additionally, Gene Ontology (GO) term enrichment analysis was performed using the clusterProfiler (v4.9.0.2) package to identify significantly enriched GO terms among the differentially expressed genes.

TRIBE and Bullseye analysis

To identify editing sites of RNA-binding proteins, a set of Perl scripts modified by the HyperTRIBE pipeline called TRIBE and Bullseye (GitHub - mflamand/Bullseye: Bullseye analysis pipeline for DART-seq analysis) were employed[43]. HyperTRIBE was utilized to identify A-to-I (A2I) mutations generated by ADAR, D1-ADAR and N3-ADAR in hPGCLCs, while Bullseye was used to identify C-to-U (C2U) mutations caused by rAPOBEC1 and D1-rAPOBEC1 in hESCs, as well as A2I mutations caused by ADAR, D1-ADAR, N3-ADAR in hESCs. To distinguish bona fide RBP binding sites from background, editing events were compared to controls expressing ADAR or rAPOBEC1 alone, ensuring retained sites were specifically enriched by RBP fusion proteins. In HyperTRIBE, the experimental group and ADAR controls were first compared to blank controls to calculate editing events. A site is recognized as an editing site if it has a minimum of 20 reads and an editing rate of 10% (number of edited reads/total reads at that site). After removing the editing sites identical to those in the ADAR controls (which are considered random editing), the remaining editing sites in the experimental group were classified as high-confidence editing sites[43]. In Bullseye, the experimental group was directly compared to ADAR/rAPOBEC controls, and sites with editing rates between 5% and 99% and editing levels higher than a certain multiple of the control cell (1.5 times for C2U and 3 times for A2I) are retained as editing sites[48]. These editing events were converted into bedgraph or bed file formats for visualization.

Identification of co-editing events. The co_editing.pl script from the Bullseye pipeline was utilized to quantify the co-editing events of ADAR and rAPOBEC1. This script identifies co-editing events as editing sites of ADAR and rAPOBEC1 found within 150 nt of each other, allowing these sites to span over one annotated intron (hg38 Geneode V36). Subsequently, BAM files of the samples were analyzed to identify co-editing pairs where at least 20 reads covered both editing sites. For each co-editing pair, the script calculates the expected co-editing rate (coeditingexp = %A2I × %C2U) and the expected number of co-editing reads (coediting readsexp = coeditingexp × coverage). Editing sites were filtered to retain those co-editing pairs with at least three edited reads at each editing site and with coediting readsexp ≥ 1 or observed co-editing reads ≥1[48].

Using RNA editing score to quantify editing of different samples. To compare editing at the RNA level, we used the RNA editing score published before[48]. The difference in editing between different samples was measured by log2[(sample1 + 1)/(sample2 + 1) +1].

Quantification and statistical analysis

In each figure legend, data are shown as the mean ± standard deviation (SD). and statistical analyses were performed using GraphPad Prism software, with p values calculated by the Student's t test, unless otherwise described.

To quantify the fluorescence intensity of SOX4 signals in confocal images of day 4 hPGCLC aggregate cryosections (Fig. 6E), an analysis was performed using ImageJ software. Individual cells were identified based on DAPI staining, and cells overlapping with OCT4 signals were defined as hPGCLCs. The fluorescence intensities of both OCT4 and SOX4 signals were measured in the hPGCLCs, and the resulting distribution was plotted. OCT4 signals served as the control.

Signal intensities of SOX4 from Western blot analysis were also quantified using ImageJ software. The intensity of each SOX4 band in Fig. 6F was measured and normalized to β-Actin bands, which served as the loading control. For the analysis in Fig. 6G, the normalized SOX4 values from the +Dox group were divided by the corresponding -Dox group values to calculate the final ratio. Statistical analysis was performed to evaluate the significance of differences in protein expression levels across the samples.

To visualize gene expression differences across experimental groups, boxplots were generated using the R programming language and ggplot2 package in Fig. 4H and Supplementary Fig. 5H. Expression data were transformed using log2(TPM + 1) for normalization. Statistical significance between groups was calculated using two-tailed unpaired t-tests, comparing experimental groups to the control.

Reporting summary

Further information on research design is available in the Nature Portfolio Reporting Summary linked to this article.

Data availability

Data supporting the findings of this study are available within the article and its Supplementary Information files and source data file. The RNA-seq data generated in this study have been deposited in the GEO repository under the accession number GSE268946, and the analyzed data (including intermediate results) can be accessed via the same repository. Source data are provided with this paper.

Code availability

Codes for reproduction of the results reported in this article are available from the GitHub repository [link: https://github.com/GUZHAOY/Chenlab-paper5]. Additionally, the code used in this study is also available on Zenodo with [https://doi.org/10.5281/zenodo.14781725].

References

1. Tang, W. W. C., Kobayashi, T., Irie, N., Dietmann, S. & Surani, M. A. Specification and epigenetic programming of the human germ line. *Nat. Rev. Genet.* **17**, 585–600 (2016).
2. Kobayashi, T. & Surani, M. A. On the origin of the human germline. *Development* **145**, dev150433 (2018).
3. Lawson, K. A. et al. Bmp4 is required for the generation of primordial germ cells in the mouse embryo. www.genesdev.org (1999).
4. Ohinata, Y. et al. Blimp1 is a critical determinant of the germ cell lineage in mice. *Nature* **436**, 207–213 (2005).
5. Ohinata, Y. et al. A signaling principle for the specification of the germ cell lineage in mice. *Cell* **137**, 571–584 (2009).
6. Saitou, M., Barton, S. C. & Surani, M. A. A molecular programme for the specification of germ cell fate in mice. www.nature.com/nature (2002).
7. Sasaki, K. et al. Robust in vitro induction of human germ cell fate from pluripotent stem cells. *Cell Stem Cell* **17**, 178–194 (2015).
8. Irie, N. et al. SOX17 is a critical specifier of human primordial germ cell fate. *Cell* **160**, 253–268 (2015).
9. Irie, N., Sybirna, A. & Surani, M. A. What can stem cell models tell us about human germ cell biology? in *Current Topics in Developmental Biology* Vol. 129, 25–65 (Academic Press Inc., 2018).
10. Magnúsdóttir, E. et al. A tripartite transcription factor network regulates primordial germ cell specification in mice. *Nat. Cell Biol.* **15**, 905–915 (2013).
11. Nakaki, F. et al. Induction of mouse germ-cell fate by transcription factors in vitro. *Nature* **501**, 222–226 (2013).
12. Campolo, F. et al. Essential role of Sox2 for the establishment and maintenance of the germ cell line. *Stem Cells* **31**, 1408–1421 (2013).
13. Chen, D. et al. The TFAP2C-regulated OCT4 naive enhancer is involved in human germline formation. *Cell Rep.* **25**, 3591–3602.e5 (2018).
14. Elliott, D. Pathways of post-transcriptional gene regulation in mammalian germ cell development. *Cytogenet Genome Res* **103**, 210–216 (2003).
15. Licatalosi, D. D. Roles of RNA-binding proteins and post-transcriptional regulation in driving male germ cell development in the mouse. *Adv. Exp. Med. Biol.* **907**, 123–151 (2016).
16. Gerstberger, S., Hafner, M. & Tuschl, T. A census of human RNA-binding proteins. *Nat. Rev. Genet.* **15**, 829–845 (2014).
17. Niimi, Y. et al. Essential role of mouse Dead end1 in the maintenance of spermatogonia. *Dev. Biol.* **445**, 103–112 (2019).
18. Ruthig, V. A. et al. A transgenic DND1GFPfusion allele reports in vivo expression and RNA-binding targets in undifferentiated mouse germ cells. *Biol. Reprod.* **104**, 861–874 (2021).
19. Yamaji, M. et al. Functional reconstruction of NANOS3 expression in the germ cell lineage by a novel transgenic reporter reveals distinct subcellular localizations of NANOS3. *Reproduction* **139**, 381–393 (2010).
20. Suzuki, H., Sada, A., Yoshida, S. & Saga, Y. The heterogeneity of spermatogonia is revealed by their topology and expression of marker proteins including the germ cell-specific proteins Nanos2 and Nanos3. *Dev. Biol.* **336**, 222–231 (2009).
21. Gassei, K. et al. DDX4-EGFP transgenic rat model for the study of germline development and spermatogenesis. *Biol. Reprod.* **96**, 707–719 (2017).
22. Hickford, D. E., Frankenberg, S., Pask, A. J., Shaw, G. & Renfree, M. B. DDX4 (VASA) is conserved in germ cell development in marsupials and monotremes. *Biol. Reprod.* **85**, 733–743 (2011).
23. Gross-Thebing, T. & Raz, E. Dead end and Detour: The function of the RNA-binding protein Dnd in posttranscriptional regulation in the germline. In *Current Topics in Developmental Biology* Vol. 140, 181–208 (Academic Press Inc., 2020).
24. Gross-Thebing, T. et al. The vertebrate protein dead end maintains primordial germ cell fate by inhibiting somatic differentiation. *Dev. Cell* **43**, 704–715.e5 (2017).
25. Suzuki, A. et al. Dead end1 is an essential partner of NANOS 2 for selective binding of target RNA s in male germ cell development. *EMBO Rep.* **17**, 37–46 (2016).
26. Hirano, T., Wright, D., Suzuki, A. & Saga, Y. A cooperative mechanism of target RNA selection via germ-cell-specific RNA-binding proteins NANOS2 and DND1. *Cell Rep.* **39**, 110894 (2022).
27. Kedde, M. et al. RNA-binding protein Dnd1 inhibits microRNA access to target mRNA. *Cell* **131**, 1273–1286 (2007).
28. Yamaji, M. et al. DND1 maintains germline stem cells via recruitment of the CCR4-NOT complex to target mRNAs. *Nature* **543**, 568–572 (2017).
29. Xie, X. et al. A homozygous missense variant in DND1 causes non-obstructive azoospermia in humans. *Front. Genet.* **13**, 1017302 (2022).
30. Mall, E. M. et al. Heading towards a dead end: the role of DND1 in germ line differentiation of human iPSCs. *PLoS ONE* **16**, e0258427 (2021).
31. Glisovic, T., Bachorik, J. L., Yong, J. & Dreyfuss, G. RNA-binding proteins and post-transcriptional gene regulation. *FEBS Lett.* **582**. https://doi.org/10.1016/j.febslet.2008.03.004 (2008).
32. Tsuda, M. et al. *Conserved Role of Nanos Proteins in Germ Cell Development*. www.sciencemag.org/cgi/content/full/301/5637/1239/.
33. Wu, X. et al. A NANOS3 mutation linked to protein degradation causes premature ovarian insufficiency. *Cell Death Dis.* **4**, e825 (2013).
34. Santos, M. G. et al. Homozygous inactivating mutation in NANOS3 in two sisters with primary ovarian insufficiency. *Biomed. Res. Int.* **2014**, 787465 (2014).
35. Youngren, K. K. et al. The Ter mutation in the dead end gene causes germ cell loss and testicular germ cell tumours. *Nature* **435**, 360–364 (2005).

36. Weidinger, G. et al. Dead end, a novel vertebrate germ plasm component, is required for zebrafish primordial germ cell migration and survival results and discussion zebrafish dead end RNA is a component of the germ plasm and is specifically expressed in primordial germ cells. *Curr. Biol.* **13**, 1429–1434 (2003).
37. Li, Q. et al. CRISPR–Cas9-mediated base-editing screening in mice identifies DND1 amino acids that are critical for primordial germ cell development. *Nat. Cell Biol.* **20**, 1315–1325 (2018).
38. Li, B. et al. A whole-mechanical method to establish human embryonic stem cell line HN4 from discarded embryos. *Cytotechnology* **62**, 509–518 (2010).
39. Chen, D. et al. Human primordial germ cells are specified from lineage-primed progenitors. *Cell Rep.* **29**, 4568–4582.e5 (2019).
40. Gu, Y. et al. Integrated analysis and systematic characterization of the regulatory network for human germline development. *J Genet Genomics*. **52**, 204–219 (2025).
41. Suzuki, H., Tsuda, M., Kiso, M. & Saga, Y. Nanos3 maintains the germ cell lineage in the mouse by suppressing both Bax-dependent and -independent apoptotic pathways. *Dev. Biol.* **318**, 133–142 (2008).
42. Jin, S. et al. Identification of SRSF3 target mRNAs using inducible TRIBE. *Biochem. Biophys. Res. Commun.* **578**, 21–27 (2021).
43. McMahon, A. C. et al. TRIBE: hijacking an RNA-editing enzyme to identify cell-specific targets of RNA-binding proteins. *Cell* **165**, 742–753 (2016).
44. Kojima, Y. et al. Evolutionarily distinctive transcriptional and signaling programs drive human germ cell lineage specification from pluripotent stem cells. *Cell Stem Cell* **21**, 517–532.e5 (2017).
45. Chen, D. et al. Germline competency of human embryonic stem cells depends on eomesodermin. *Biol. Reprod.* **97**, 850–861 (2017).
46. Brannan, K. W. et al. Robust single-cell discovery of RNA targets of RNA-binding proteins and ribosomes. *Nat. Methods* **18**, 507–519 (2021).
47. Owens, M. C. & Liu, K. F. TRIBE-STAMP reveals new insights into the functions of RNA binding proteins. *Genes Dev.* **36**, 954–955 (2022).
48. Flamand, M. N., Ke, K., Tamming, R. & Meyer, K. D. Single-molecule identification of the target RNAs of different RNA binding proteins simultaneously in cells. *Genes Dev.* **36**, 1002–1015 (2022).
49. Gebauer, F., Preiss, T. & Hentze, M. W. From cis-regulatory elements to complex RNPs and back. *Cold Spring Harb. Perspect. Biol.* **4**, a012245 (2012).
50. Roy, B. & von Arnim, A. G. Translational Regulation of Cytoplasmic mRNAs. *Arabidopsis Book* **11**, e0165 (2013).
51. Radford, H. E., Meijer, H. A. & de Moor, C. H. Translational control by cytoplasmic polyadenylation in Xenopus oocytes. *Biochim. Biophys. Acta* **1779**, https://doi.org/10.1016/j.bbagrm.2008.02.002 (2008).
52. Winata, C. L. & Korzh, V. The translational regulation of maternal mRNAs in time and space. *FEBS Lett.* **592**, https://doi.org/10.1002/1873-3468.13183 (2018).
53. Hu, Y. et al. Enhanced single RNA imaging reveals dynamic gene expression in live animals. *Elife* **12**, e82178 (2023).
54. Waghray, S., Williams, C., Coon, J. J. & Wickens, M. Xenopus CAF1 requires NOT1-mediated interaction with 4E-T to repress translation in vivo. *RNA* **21**, 1335–1345 (2015).
55. Gu, Y. et al. Integrated analysis and systematic characterization of the regulatory network for human germline development. *J. Genet. Genom.* https://doi.org/10.1016/j.jgg.2024.11.005 (2024).
56. Angeles Julaton, V. T. & Reijo Pera, R. A. NANOS3 function in human germ cell development. *Hum. Mol. Genet.* **20**, 2238–2250 (2011).
57. Saga, Y. Function of Nanos2 in the male germ cell lineage in mice. *Cell. Mol. Life Sci.* **67**, https://doi.org/10.1007/s00018-010-0456-x (2010).
58. Zhao, N. et al. Targeting eIF4A triggers an interferon response to synergize with chemotherapy and suppress triple-negative breast cancer. *J. Clin. Investig.* **133**, e172503 (2023).
59. Tang, W. W. C. et al. Sequential enhancer state remodelling defines human germline competence and specification. *Nat. Cell Biol.* **24**, 448–460 (2022).
60. Zhang, J. et al. OTX2 restricts entry to the mouse germline. *Nature* **562**, 595–599 (2018).
61. Siddiqui, N. U. et al. Smaug regulates germ plasm assembly and primordial germ cell number in drosophila embryos. *Sci. Adv.* **10**, eadg7894 (2024).
62. Chen, R., Stainier, W., Dufourt, J., Lagha, M. & Lehmann, R. Direct observation of translational activation by a ribonucleoprotein granule. *Nat. Cell Biol.* **26**, 1322–1335 (2024).
63. Sybirna, A., Wong, F. C. K. & Surani, M. A. Genetic basis for primordial germ cells specification in mouse and human: conserved and divergent roles of PRDM and SOX transcription factors. In *Current Topics in Developmental Biology* Vol. 135, 35–89 (Academic Press Inc., 2019).
64. Noguchi, T. & Noguchi, M. A recessive mutation (ter) causing germ cell deficiency and a high incidence of congenital testicular teratomas in 129/Sv-ter mice. *J. Natl. Cancer Inst.* **75**, 385–392 (1985).
65. Cook, M. S., Coveney, D., Batchvarov, I., Nadeau, J. H. & Capel, B. BAX-mediated cell death affects early germ cell loss and incidence of testicular teratomas in Dnd1Ter/Ter mice. *Dev. Biol.* **328**, 377–383 (2009).
66. Hubstenberger, A. et al. P-body purification reveals the condensation of repressed mRNA regulons. *Mol. Cell* **68**, 144–157.e5 (2017).
67. Luo, Y., Na, Z. & Slavoff, S. A. P-Bodies: composition, properties, and functions. *Biochemistry* **57**, https://doi.org/10.1021/acs.biochem.7b01162 (2018).
68. Youn, J. Y. et al. Properties of stress granule and P-Body proteomes. *Mol. Cell* **76**, https://doi.org/10.1016/j.molcel.2019.09.014 (2019).
69. Di Stefano, B. et al. The RNA helicase DDX6 controls cellular plasticity by modulating P-Body homeostasis. *Cell Stem Cell* **25**, 622–638.e13 (2019).
70. Wu, B., Eliscovich, C., Yoon, Y. J. & Singer, R. H. Translation dynamics of single mRNAs in live cells and neurons. *Science* **352**, 1430–1435 (2016).
71. Shan, T. et al. m6A modification negatively regulates translation by switching mRNA from polysome to P-body via IGF2BP3. *Mol. Cell* **83**, 4494–4508.e6 (2023).
72. Horlbeck, M. A. et al. Compact and highly active next-generation libraries for CRISPR-mediated gene repression and activation. *Elife* **5**, e19760 (2016).

Acknowledgements

We thank the Core Facility of Zhejiang University-University of Edinburgh (ZJE) Institute, the Biomed-X Laboratory of ZJE Institute, School of Medicine, Zhejiang University, for continuous support. This work was supported by the National Natural Science Foundation of China awarded to D.C. (Grant No. 32270835), Zhejiang Natural Science Foundation, awarded to D.C. (Grant No. Z22C129553), and National Key R&D Program of China, awarded to D.C. (Grant No. 2024YFA1108100).

Author contributions

D.C., Z.W., and H.Y. conceived the study, designed the experiments, and wrote the manuscript. Z.W. and H.Y. performed most of the experiments. Z.G. and Y.Y. performed bioinformatics analysis. X.S. (Xiaohui Shi), Y.J., Y.L, and H.L. performed western blot and co-IP experiments. Q.S. performed library construction for low-cell RNA sequencing. J.M., Y.X., and W.L. participated in construction of knockout cell lines. J.M., J.D., Q.L., J.S., and R.Q. participated in the construction of overexpression and knockdown related cell lines. X.S. (Xinchen Shen) and W.H. provided assistance in the induction of hPGCLCs. D.C., M.B., Z.W., H.Y., Z.G., Y.Y., S.Y., M.J., and Y.G. participated in the review and revision of the manuscript.

Competing interests
The authors declare no competing interests.

Additional information
Supplementary information The online version contains supplementary material available at https://doi.org/10.1038/s41467-025-57490-6.

Correspondence and requests for materials should be addressed to Matthew Brook or Di Chen.

Peer review information *Nature Communications* thanks Blanche Capel, who co-reviewed with Talia Hatkevich; Stefan Schlatt, and the other, anonymous, reviewer(s) for their contribution to the peer review of this work. A peer review file is available.